
Path-conditioned training: a principled way to rescale ReLU neural networks

Arthur Lebeurier¹ Titouan Vayer² Remi Gribonval³

Abstract

Despite recent algorithmic advances, we still lack principled ways to leverage the well-documented rescaling symmetries in ReLU neural network parameters. While two properly rescaled weights implement the same function, the training dynamics can be dramatically different. To offer a fresh perspective on exploiting this phenomenon, we build on the recent path-lifting framework, which provides a compact factorization of ReLU networks. We introduce a geometrically motivated criterion to rescale neural network parameters which minimization leads to a conditioning strategy that aligns a kernel in the path-lifting space with a chosen reference. We derive an efficient algorithm to perform this alignment. In the context of random network initialization, we analyze how the architecture and the initialization scale jointly impact the output of the proposed method. Numerical experiments illustrate its potential to speed up training.

1. Introduction

Deep learning has become the dominant paradigm in machine learning, with neural networks achieving breakthrough performance across vision, language, and scientific domains. Training these networks represents a central computational challenge, particularly for large language models where the cost approximately doubles every 6 months (Sastry et al., 2024). Addressing this challenge requires progress on two fronts: (1) a better understanding of the optimization dynamics, and (2) translating these insights into practical improvements for state-of-the-art models.

¹ENS de Lyon, CNRS, Inria, Université Claude Bernard Lyon 1, LIP, UMR 5668, 69342, Lyon cedex 07, France ²Inria, Rennes, France ³Inria, CNRS, ENS de Lyon, Université Claude Bernard Lyon 1, LIP, UMR 5668, 69342, Lyon cedex 07, France. Correspondence to: Arthur Lebeurier <arthur.lebeurier@ens-lyon.fr>.

Preprint. February 24, 2026.

Code available at <https://github.com/Artim436/pathcond>

Among all neural network architectures, ReLU networks play a singular role, as they have demonstrated strong empirical performance over the years on a lot of tasks (Krizhevsky et al., 2012; Szegedy et al., 2015; Howard et al., 2017; Silver et al., 2016; Dosovitskiy et al., 2021). Importantly, ReLU networks exhibit a well-documented symmetry: specific weights rescaling leave the network function unchanged due to the positive homogeneity of the ReLU activation. This symmetry has many implications.

First, it has proven useful in understanding existing optimization algorithms through conservation laws and implicit biases (Du et al., 2018; Kunin et al., 2021; Marcotte et al., 2023; Zhao et al., 2023). In short, these analyses reveal conserved quantities, arising for example from the rescaling symmetry, that constrain and shape the geometry of learning trajectories in both parameter and function space. These effects are closely related to the so-called “rich feature regime” in which the network learns “meaningful” representations from the data (Kunin et al., 2024; Dominé et al., 2025). Moreover, it has been shown that the implicit bias of gradient-based optimization can be characterized through a mirror-flow reparameterization of the dynamics (Gunasekar et al., 2018; Azulay et al., 2021), which can be understood, in part, by leveraging the rescaling symmetry of ReLU networks (Marcotte et al., 2025).

Second, rescaling symmetry has enabled the design of novel optimization methods that exploit this invariance to either accelerate training or reach better local minima. Notable examples include \mathcal{G} -SGD (Meng et al., 2019), Path-SGD (Neyshabur et al., 2015), and Equinormalization (Stock et al., 2019), among others (Badrinarayanan et al., 2015; Saul, 2023b; Mustafa & Burkholz, 2024). Broadly, these methods can be categorized into two groups: *teleportation* approaches (Zhao et al., 2022; Armenta et al., 2023), which perform a standard optimization step followed by a “symmetry-aware” correction that preserves the implemented function, and algorithms that are intrinsically invariant to the underlying symmetries.

However, the problem of leveraging rescaling symmetries to better understand and improve training dynamics remains open, as the previously mentioned schemes are often guided more by practical considerations than by formal theoretical principles. In this context, the objective of this article is

to leverage the concept of path-lifting Φ (Neysshabur et al., 2015; Bona-Pellissier et al., 2022; Stock & Gribonval, 2023; Gonon et al., 2023) in a geometrically motivated manner to design algorithms that improve training dynamics. The path-lifting $\Phi(\theta)$ provides an intermediate representation between the finite-dimensional parameter space θ (weights and biases) and the infinite-dimensional space of network realizations f_θ (the functions implemented by the network).

Contributions and outline. After developing a geometric perspective based on path-lifting that clarifies the role of rescaling symmetries in neural network training dynamics, we propose a new geometry-aware rescaling criterion to “teleport” any given parameter θ by a rescaling-equivalent one θ' with better training properties, as well as an efficient algorithm to compute θ' , called `PathCond`. We provide a thorough analysis of the effects of our criterion, establishing regimes of interest in terms of initialization scale and architectural choices. We demonstrate that on specific datasets and architectures, using our (parameter free) rescaling criterion at initialization alone can significantly improve training dynamics, and never degrades it. On CIFAR-10, we show that we can achieve the same accuracy as the baseline in $1.5\times$ fewer epochs.

Notations. The data dimension will be denoted by d , the output dimension by k , parameters of the neural network will be in \mathbb{R}^p and the lifted representation in \mathbb{R}^q . The networks will have H neurons.

2. Sketch of the idea on a simple example

To illustrate the overall approach considered in this paper, let us start with a standard problem where we have access to n training data (x_i, y_i) with $x_i \in \mathbb{R}^d, y_i \in \mathbb{R}^k$, and, given a loss we wish to find a parametrized function (typically a neural network) $f_\theta : \mathbb{R}^d \rightarrow \mathbb{R}^k$ with $\theta \in \mathbb{R}^p$ that minimizes $L(\theta) := \frac{1}{n} \sum_{i=1}^n \text{loss}(f_\theta(x_i), y_i)$. To give intuition about our method, we place ourselves in the idealized scenario where the optimization is carried via a gradient flow

$$\dot{\theta} = -\nabla L(\theta). \quad (1)$$

From parameter space to lifted space. Consider the simplest ReLU setting where $H = d = k = 1$ and f_θ is a one-neuron ReLU network with bias $f_{\theta=(u,v,w)}(x) = u \text{ReLU}(vx + w)$. The rescaling invariance property manifests itself via the fact that, for each $\lambda > 0$, the rescaled parameter $\theta^{(\lambda)} := (\frac{1}{\lambda}u, \lambda v, \lambda w)$ satisfies $f_\theta = f_{\theta^{(\lambda)}}$. This function rewrites as $f_\theta(x) = u \mathbf{1}_{vx+w>0}(vx + w)$, that is, $f_\theta(x) = \mathbf{1}_{vx+w>0} \langle \Phi(\theta), \begin{pmatrix} x \\ 1 \end{pmatrix} \rangle$ where $\Phi(\theta) = (uv, uw)^\top$.

One important property of the vector $\Phi(\theta)$, called the path-lifting (formal definition in Section 3), is its rescaling in-

so that $f_{\theta'} = f_\theta$

variance property: $\Phi(\theta) = \Phi(\theta^{(\lambda)})$ for any $\lambda > 0$. In other words, if we rescale the input parameters by $\lambda > 0$ and the output parameter by $1/\lambda$ we do not change f_θ and $\Phi(\theta)$. In particular for a parameter vector $\theta = (u, v, w)$ with $u > 0$, rescaling with $\lambda := u$ yields that for every input x we have $f_\theta(x) = f_{\theta^{(u)}}(x) = \text{ReLU}(\langle \Phi(\theta), \begin{pmatrix} x \\ 1 \end{pmatrix} \rangle)$, i.e., f_θ only depends on $\Phi(\theta)$.

With $\theta_{\text{opt}} = (1, 1, 0)^\top$, $f_{\theta_{\text{opt}}} = \text{ReLU}$, and if we sample $x_i \sim \mathcal{N}(0, 1), y_i = f_{\theta_{\text{opt}}}(x_i) = \text{ReLU}(x_i)$, and train with the square loss, the previous discussion leads to two conclusions. First, the risk $L(\theta)$ only depends on $\Phi(\theta)$ when $u > 0$, it can be factorized as $L(\theta) = \ell(\Phi(\theta))$. Second, any model f_θ satisfying $\Phi(\theta) = \Phi(\theta_{\text{opt}}) = (1, 0)^\top$ implements the same function ReLU and achieves zero training loss. This motivates an approach in which the learning problem is viewed not only as optimization over θ in parameter space, *but also as optimization in the lifted space over $\Phi(\theta)$, where targeting $\Phi_{\text{opt}} := \Phi(\theta_{\text{opt}})$ provides a principled strategy from the perspective of minimizing the training loss.*

Rescaling to mimic gradient descent in lifted space. The overall approach of this paper is thus guided by a geometric view of the training dynamics *in a lifted representation of the network*. This can be illustrated on our simple example by minimizing $L(\theta)$ with standard gradient descent (GD) and small learning rates (simulating the gradient flow (1)), and observing it both in parameter space and in lifted space, for different initializations (Figure 1). By the chain rule, the ODE (1) also induces an ODE in the lifted space: denoting $P_\theta := \partial\Phi(\theta)\partial\Phi(\theta)^\top$ the *path-kernel*,

$$\partial_t \Phi(\theta) := \frac{d}{dt} \Phi(\theta(t)) = -P_\theta \nabla_{\Phi} \ell(\Phi(\theta)). \quad (2)$$

The rescaling invariance of $\Phi(\theta)$ *does not extend to the path kernel P_θ* : the latter varies when θ is replaced by $\theta^{(\lambda)}$. As described later, given θ , `PathCond` aims to identify a parameter rescaling λ such that $\theta' := \theta^{(\lambda)}$ somehow *conditions* the path kernel $P_{\theta'}$, i.e. best aligns it with the identity so that $P_{\theta'} \approx I$. This alignment aims to induce trajectories in lifted space close to those that would have been achieved by directly performing gradient descent / flow in the lifted space $\dot{\Phi} \approx -\nabla \ell(\Phi)$, without ever incurring the cost of pseudo-inverting large matrices appearing in “natural gradient” approaches (see discussion in Appendix B).

For our example, such rescaling factors are computed using `PathCond` for three considered initializations, and the resulting trajectories of $(\theta(t), \Phi(\theta(t)))$ are illustrated in Figure 1. As shown in the left subplot, rescaled initializations (plain lines) lead to faster convergence, and indeed, as illustrated in the middle subplot, the trajectories

In general, $f_\theta(x) = \text{sign}(u) \text{ReLU}(\text{sign}(u) \langle \Phi(\theta), (x, 1)^\top \rangle)$, so f_θ only depends on $\text{sign}(\theta), \Phi(\theta)$.

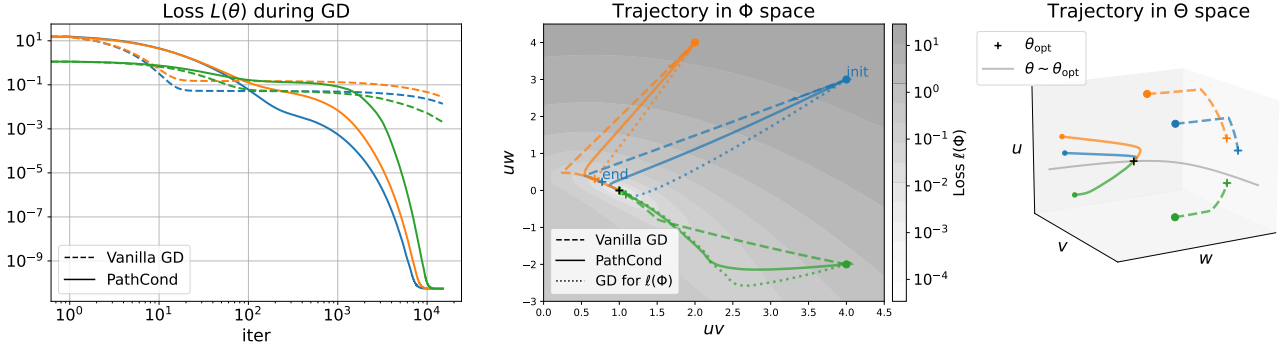


Figure 1. GD for a toy model $f_{\theta=(u,v,w)}(x) = u \text{ReLU}(vx+w)$ on a loss $L(\theta)$ that can be factorized as $L(\theta) = \ell(\Phi(\theta))$ (see Section 2). (Left) Loss $L(\theta)$ during GD iterations for three different initializations θ_0 (three colors). Dashed lines correspond to GD starting at θ_0 , bold lines to GD starting at rescaled $\theta_0^{(\lambda)} \sim \theta_0$ using PathCond; (Middle) Trajectories in lifted space $\Phi(\theta) = (uv, uw)^\top$. Dotted lines are trajectories corresponding to $\partial_t \Phi = -\nabla_{\Phi} \ell(\Phi)$ (GD on $\ell(\Phi)$). (Right) Trajectories in parameter space.

in lifted space obtained with rescaled initializations (bold lines) more closely follow the trajectory of the idealized ODE $\partial_t \Phi = -\nabla_{\Phi} \ell(\Phi)$ (dotted lines) than the trajectories starting from the non-rescaled initializations (dashed lines).

Relation to (neural tangent) kernel conditioning. The general approach described in the next section builds on the vision that the insights drawn from the above simple example, as well as the underlying motivations, extend to larger-scale models. Before entering into the details, let us briefly explain how the resulting approach also bears connections with the conditioning of the celebrated neural tangent kernel (NTK) (Jacot et al., 2018).

As described in many contexts, the dynamic in (1) also induces an ODE on $f_{\theta(t)}(x)$ (at any point x) driven by the NTK $K_{\theta}(x, x') := \partial_{\theta} f_{\theta}(x) \partial_{\theta} f_{\theta}(x')^\top \in \mathbb{R}^{k \times k}$ (Jacot et al., 2018) where $\partial_{\theta} f_{\theta}(x) \in \mathbb{R}^{k \times p}$ denotes the Jacobian of $\theta \rightarrow f_{\theta}(x)$. The NTK can be used to analyze the dynamics of neural networks in specific training regimes. In particular, the spectrum of the NTK governs the convergence rate of the training loss (Bowman, 2023); for instance, larger NTK eigenvalues in certain over-parameterized (lazy) regimes—corresponding to linearized networks (Chizat et al., 2019)—lead to faster convergence rates (Jacot et al., 2018; Arora et al., 2019).

As already observed by Gebhart et al. (2021); Patil & Dvornik (2021), when applying the general path-lifting framework to ReLU networks, the NTK admits a factorization that separates the architectural contribution from a data-dependent term:

$$K_{\theta}(x, x') = Z(x, \theta) P_{\theta} Z(x', \theta)^\top, \quad (3)$$

where $P_{\theta} = \partial \Phi(\theta) \partial \Phi(\theta)^\top$ is the previously introduced path-kernel and $Z(x, \theta)$ depends on the activations at every ReLU neuron. Equation (3) suggests that modifying the spectral properties of P_{θ} , for instance through appropriate changes on θ , can improve the training dynamics, and that

such modifications can be performed solely based on the network architecture via $\Phi(\theta)$, i.e., *independently of the data*. For example, in the context of parameter pruning, Patil & Dvornik (2021) exploit this decomposition to select a subset of parameters that maximizes the trace of P_{θ} within the subnetwork. In contrast, our approach PathCond focuses on improving the conditioning of P_{θ} *without altering the function f_{θ}* , by applying an efficiently chosen rescaling based on a principled criterion.

3. Rescaling symmetries and the path-lifting

In this section, we introduce the tools underlying our method PathCond, which builds upon the rescaling symmetries of ReLU networks and the path-lifting framework.

Rescaling equivalent parameters. As advertised in Section 2, for any neuron in a ReLU network, we can scale its incoming weights by a factor $\lambda > 0$ and simultaneously scale its outgoing weights by $1/\lambda$ without changing the neuron’s input-output mapping (Neyshabur et al., 2015; Dinh et al., 2017). This corresponds to multiplying the parameter vector θ by a certain *admissible* diagonal matrix $D \in \mathcal{D}$ with positive entries. Formally, denoting \mathcal{D} the multiplicative group generated by the set of all such diagonal matrices (when both the chosen neuron and the factor λ vary), two parameter vectors θ and θ' are said to be rescaling equivalent (denoted $\theta' \sim \theta$) if there is $D \in \mathcal{D}$ such that $\theta' = D\theta$ (see details in Appendix D). This defines an equivalence relation on the parameter space, partitioning it into equivalence classes. Importantly, when θ, θ' belong to the same class we have $f_{\theta'} = f_{\theta}$.

Gradient flow is not rescaling invariant. Crucially, gradient flow does *not* respect this symmetry: rescaling-equivalent parameters $\theta \sim \theta'$ used at initialization of the gradient flow (1) generally lead to different trajectories. This lack of invariance has profound implications. For instance,

unbalanced parameter initializations—obtained by applying extreme rescalings (with $\lambda \gg 1$ or $\lambda \ll 1$ for each neuron) to a balanced initialization—can lead to arbitrarily poor optimization and generalization performance (Neyshabur et al., 2015). Conversely, this sensitivity can be exploited: by carefully controlling the rescaling structure, we can hope to guide the training dynamics toward more favorable trajectories (as illustrated in Figure 1). While these ideas have been exploited through several heuristics, which we will review below, our goal is to design a more *principled* heuristic.

Path-lifting. The path lifting framework (Neyshabur et al., 2015; Bona-Pellissier et al., 2022; Gonon et al., 2023) factors out the parameter redundancy induced by rescaling symmetries. This is achieved through a lifting map Φ from \mathbb{R}^p to a lifted space \mathbb{R}^q that captures the essential geometric structure of the network while eliminating redundant degrees of freedom. For any parameter θ and path p , the p -th entry of $\Phi(\theta)$ writes $\prod_{i \in p} \theta_i$, i.e., is the product of the weights along the path. Interestingly, for any output neuron v_{out} of f_θ , we can compactly write

$$v_{\text{out}}(\theta; x) = \left\langle \Phi(\theta), A_{v_{\text{out}}}(\theta, x) \begin{pmatrix} x \\ 1 \end{pmatrix} \right\rangle, \quad (4)$$

where $A_{v_{\text{out}}}(\theta, x)$ is a binary-valued matrix capturing the data-dependent activation patterns (this generalizes the toy example of Section 2). Two of the key properties of Φ are: a) rescaling-equivalent parameters have the same lifted representation:

$$\Phi(\theta) = \Phi(D\theta), \quad \forall D \in \mathcal{D}. \quad (5)$$

and b) it induces a (local) factorization of the global loss.

$$\forall \theta \in \Omega \subset \mathbb{R}^p, \quad L(\theta) = \ell(\Phi(\theta)), \quad (6)$$

for some $\ell : \mathbb{R}^q \rightarrow \mathbb{R}$, enabling the analysis of the dynamics in the lifted space rather than the redundant parameter space (Stock & Gribonval, 2023; Marcotte et al., 2025).

4. Path-conditioned training

Using the local factorization of the loss (6), the starting point of our analysis is that, by the chain rule, the variable $z(t) := \Phi(\theta(t))$ in lifted space \mathbb{R}^q satisfies

$$\begin{aligned} \dot{z}(t) &= \partial\Phi(\theta(t))\dot{\theta}(t) = -\partial\Phi(\theta(t))\partial\Phi(\theta(t))^\top \nabla\ell(z(t)) \\ &= -P_{\theta(t)} \nabla\ell(z(t)) \end{aligned} \quad (7)$$

as soon as the variable $\theta(t)$ in parameter space \mathbb{R}^p satisfies (1). The *path-kernel* $P_\theta = \partial\Phi(\theta)\partial\Phi(\theta)^\top \in \mathbb{R}^{q \times q}$ (Gebhart et al., 2021; Marcotte et al., 2025) is thus a (local)

metric tensor that encodes how parameter updates propagate in the lifted space \mathbb{R}^q . This shows that (1), the gradient flow in parameter space \mathbb{R}^p , induces a preconditioned flow in the lifted space \mathbb{R}^q , with preconditioner equal to P_θ . This can be put in perspective with natural gradient approaches (Amari, 1998; Martens, 2020), where the geometry is induced by the Fisher information matrix, whereas in our setting it is shaped by the path kernel.

4.1. Rescaling is pre-conditioning

If we replace a parameter θ (either at initialization or during training iterations) by a rescaled version $\theta' = D\theta$, $D \in \mathcal{D}$, then since $z = \Phi(\theta)$ is unchanged, only P_θ on the right-hand-side of (7) can depend on D . In other words, *selecting some admissible rescaling corresponds to shaping the geometry of the optimization dynamics in the lifted space*.

However, what criterion should guide the choice of a rescaling? Several heuristic approaches exist: Equinormalization (Stock et al., 2019; Saul, 2023a) explicitly chooses D to minimize some $\ell_{p,q}$ norm of $\theta' = D\theta$ or Mustafa & Burkholz (2024) select rescalings that promote more balanced weights across successive layers (for graph attention networks).

We show in Appendix C that on toy examples several natural criteria used in the literature are in fact equivalent: the Euclidean norms $\|\theta'\|_2$ and $\|\nabla L(\theta')\|_2$, the condition number $\kappa(\nabla^2 L(\theta'))$, the trace $\text{tr}(\nabla^2 L(\theta'))$, or the operator norm $\|\nabla^2 L(\theta')\|_{2 \rightarrow 2}$. However, this no longer holds for larger models, and an appropriate criterion must be selected.

4.2. Proposed rescaling criterion

Rather than the heuristic criteria to choose D described above, PathCond relies on a criterion defined by the path kernel. Our strategy is based on the assumption that *gradient descent in the lifted space provides a suitable, rescaling-invariant idealized trajectory*. Accordingly, the rescaling D is chosen to mimic this behavior by seeking to *best align* $P_{D\theta} \nabla\ell(\Phi(\theta)) \in \mathbb{R}^q$ with $\nabla\ell(\Phi(\theta)) \in \mathbb{R}^q$. A first naive approach would attempt to actually compute $\nabla\ell(\Phi(\theta))$ and optimize some correlation with $P_{D\theta} \nabla\ell(\Phi(\theta))$. This would however be highly impractical for practical networks as the dimension q of these vectors is the number of *paths* in the graph associated to the network, which grows combinatorially with the network size (e.g., it is in the order of $q = 10^{58}$ for ResNet18, details in Appendix D).

Instead, we propose to directly seek an alignment between P_θ and the identity matrix. As before, a naive attempt to explicitly compute and optimize $P_\theta \in \mathbb{R}^{q \times q}$ is computationally infeasible. However, as we show next, a carefully designed criterion enables us to entirely bypass this bottleneck: we identify optimal rescalings—according to the

A sequence of edges from some neuron to an output neuron.

In the simple example given in Section 2, one possible choice of Ω corresponds the region $u > 0$.

Algorithm 1 Idealized Rescaling Algorithm

- 1: **Input:** Learning rates $(\mu_k)_{k \geq 0}$, loss function $L(\cdot)$, divergence $d(\cdot|\cdot)$.
- 2: Iterate following or only teleport initialization.
- 3: **for** $k = 0, 1, 2, \dots$ **do**
- 4: $(\alpha_k, D_k) = \operatorname{argmin}_{\alpha > 0, D \in \mathcal{D}} d(\alpha G_{D\theta_k} || I_p)$ // see Algorithm 2
- 5: Set $\theta_{k+\frac{1}{2}} = D_k \theta_k$ // Teleportation step
- 6: $\theta_{k+1} = \theta_{k+\frac{1}{2}} - \mu_k \nabla L(\theta_{k+\frac{1}{2}})$ // Gradient step
- 7: **end for**

proposed criterion—*without ever forming or storing* P_θ . To this end, we must address two challenges: *how to measure the “distance” between P_θ and the identity matrix I , and how to circumvent the computational bottleneck arising from the combinatorial size $q \times q$ of P_θ .*

To address the first challenge, we use Bregman matrix divergences $d_\zeta(X||Y)$, induced by a strictly convex function ζ (Kulis et al., 2009), which provide a principled geometry on the space of symmetric matrices (see Appendix E for a formal definition). In particular, we focus on *spectral divergences*, a subclass defined via functions of the eigenvalues, encompassing common choices such as the Frobenius and logdet (James et al., 1961) divergences.

For the second question, we note that P_θ can be expressed as $P_\theta = AA^\top$, where $A = \partial\Phi(\theta)$. Using any divergence satisfying the property $d(AA^\top || I_q) = d(A^\top A || I_p)$ for every $q \times p$ matrix A , we will be able to work with the matrix $G_\theta := A^\top A = \partial\Phi(\theta)^\top \partial\Phi(\theta)$, which has size $p \times p$, with p the number of parameters. In typical neural networks, we have $p \ll q$, making G_θ significantly more manageable than P_θ . As written in Appendix E, the above property is satisfied with spectral divergences, as AA^\top and $A^\top A$ share the same spectrum.

Generic conditioning algorithm. Given such a spectral-based divergence measure $d(\cdot|\cdot)$, the above viewpoint combined with the teleportation-based algorithm of Zhao et al. (2022), leads to Algorithm 1. Note that we add a coefficient α_k in the optimization step to manage the relative scale of the kernel with respect to the identity matrix.

4.3. Explicit algorithm with the logdet divergence

The final step is to select an appropriate divergence. We choose the Bregman divergence induced by $\zeta(X) = -\log \det(X)$, defined on positive semi-definite matrices. In light of this, we focus on the optimization problem

$$\min_{D \in \mathcal{G}, \alpha > 0} d_{-\log \det}(\alpha G_{D\theta} || I_p). \quad (8)$$

With our final criterion, only the diagonal of G_θ is required.

Interestingly, $d_{-\log \det}(X||I)$ provides an upper bound on the condition number of X (Dhillon, 2008; Bock & Andersen, 2025), further supporting the interpretation of our approach as selecting a rescaling that improves the condition number of the path kernel.

To handle potential issues arising from zero eigenvalues, we consider in Appendix F a slight variation that employs the generalized determinant in place of the standard det. Furthermore, as shown in Appendix F, if $G := G_\theta$ is positive definite, that is when $\partial\Phi$ is full rank, then $G_{D\theta}$ remains positive definite for every $D \in \mathcal{D}$, and the resulting optimization problem coincides with the formulation using the standard log det. The latter can be rewritten as (Lemma F.3)

$$\min_{u \in \mathbb{R}^H} F(u) := p \log \left(\sum_{i=1}^p e^{(Bu)_i} G_{ii} \right) - \sum_{i=1}^p (Bu)_i, \quad (9)$$

where H is the number of hidden neurons, and $B \in \mathbb{R}^{p \times H}$ is a matrix with entries in $\{1, -1, 0\}$, indicating whether a parameter enters (-1), leaves (1), or is unrelated to (0) a given neuron. Each column of B corresponding to a neuron $h \in H$ takes the form $b_h = (1_{\text{out}_h}, -1_{\text{in}_h}, 0_{\text{other}_h})^\top \in \mathbb{R}^p$ (up to a permutation of coordinates), where out_h , in_h , and other_h are defined formally in Theorem D.1. The rescaling of h is given by $\lambda_h = e^{u_h}$ and $D = e^{Bu}$ (the exponential is taken entrywise) describes the overall rescaling on all parameters. As shown in Lemma F.6 in appendix, F is convex and (9) admits a solution as soon as $g := \text{diag}(G) > 0$. Although G is generally only positive *semi*-definite ($g \geq 0$), we nonetheless adopt (9) as the basis for our concrete criterion.

Indeed, the reformulation (9) presents several practical advantages. First, the objective F is defined in dimension H , corresponding to the number of neurons, which is typically much smaller than the number of parameters p . Moreover, F depends only on $g = \text{diag}(G)$ and therefore does not require the explicit computation of the full $p \times p$ matrix G_θ . The vector g can be itself computed efficiently using automatic differentiation using a single backward pass on the network (see Appendix G). Finally, (9) can be solved efficiently via alternating minimization as described below.

Lemma 4.1. *If $g > 0$, for any neuron h the problem $\min_{u_h \in \mathbb{R}} F(u_1, \dots, u_h, \dots, u_H)$ has a solution given by $\log(r_h)$ where r_h is the unique positive root of the polynomial $\mathcal{B}(\mathcal{A} + p)X^2 + \mathcal{A}DX + \mathcal{C}(\mathcal{A} - p)$ where, with $\rho_{i,h} := e^{(Bu)_i - B_{ih}u_h}$, we consider*

$$\begin{aligned} \mathcal{A} &:= |\{i \in \text{in}_h\}| - |\{i \in \text{out}_h\}|, \quad \mathcal{B} := \sum_{i \in \text{out}_h} \rho_{i,h} g_i \\ \mathcal{C} &:= \sum_{i \in \text{in}_h} \rho_{i,h} g_i, \quad \mathcal{D} := \sum_{i \in \text{other}_h} \rho_{i,h} g_i. \end{aligned}$$

We provide a detailed proof of this lemma in Appendix F.

Algorithm 2 PathCond : Path-conditioned rescaling

input : DAG ReLU network, θ to rescale
 1 $u^{(0)} = 0 \in \mathbb{R}^H$
 2 **for** $k = 0, \dots, n_{\text{iter}}$ **do**
 3 **for** each neuron h **do**
 4 Given $u^{(k)}$ compute $\mathcal{A}, \mathcal{B}, \mathcal{C}, \mathcal{D}$ defined in Lemma 4.1.
 5 Solve $r_h = \text{find_positive_root}(\mathcal{B}(\mathcal{A} + p)X^2 + \mathcal{A}\mathcal{D}X + \mathcal{C}(\mathcal{A} - p)) > 0$.
 6 $u_h^{(k+1)} = \log(r_h)$
output : Rescaled $D\theta$ where $D = \text{diag}(e^{Bu^{(n_{\text{iter}})}})$

Based on this result, we use alternating minimization with closed-form coordinate updates, yielding Algorithm 2.

Computational complexity. Algorithm 2 has time complexity $O(n_{\text{iter}}p)$ and space complexity $O(p + H)$. In practice, $n_{\text{iter}} \ll p$ with typical convergence in fewer than 10 iterations. Indeed, the computation of $\text{diag}(G)$ requires one backward pass at cost $O(p)$. We never compute Bu explicitly: at the first iteration $Bu = u = 0$, and thereafter we incrementally update Bu by adding the coefficient difference at cost $|\text{out}_h| + |\text{in}_h|$ per iteration. Each iteration cycles through H neurons, where updating neuron h costs $O(|\text{out}_h| + |\text{in}_h|)$. Since $\sum_{h=1}^H (|\text{out}_h| + |\text{in}_h|) \approx 2p$, each iteration has complexity $O(p)$. The algorithm stores dual variables $Bu \in \mathbb{R}^p$, primal variables $u \in \mathbb{R}^H$, and a sparse matrix B with $\approx 2p$ nonzero coefficients (all ± 1), and index tensors for edge sets, yielding space complexity $O(p + H)$. Full implementation details and pseudocode are provided in Section H.

5. Experiments

In this section, we demonstrate that rescaling *only at initialization* with PathCond improves training dynamics by accelerating training loss convergence. In a nutshell PathCond enables us to reach the same accuracy with up to 1.5 times less epochs without compromising generalization (Figure 3). We also compare our approach with the baseline GD with standard initialization without any rescaling, and the Equinormalization heuristic (Stock et al., 2019) (ENorm), which performs rescaling at every iteration to minimize a weighted $\ell_{2,2}$ norm of the layer weights. Unlike the ENorm criterion and its variants (Saul, 2023a), which require tuning of hyper parameters (the choice of p, q and of the weights), the PathCond criterion has no hyperparameter. Full details of the ENorm configuration used in our experiments are provided in Section N. Finally, we characterize theoretically the favorable regimes for PathCond and validate them on MNIST autoencoders (Figure 5).

5.1. Faster Training Dynamics

Training setup. Following the experimental protocol of Stock et al. (2019), we evaluate our method on fully connected networks for CIFAR-10 classification. The models take flattened 3072-dimensional images as input. The architecture consists of an initial linear layer (3072×500), followed by $L - 1$ hidden layers of size 500×500 , and a final classification layer (500×10). We vary the depth L from 3 to 9 to analyze depth-dependent effects. All weights are initialized using Kaiming uniform initialization (He et al., 2015). We do 100 epochs of SGD, with a batch size of 128 and a fixed learning rate (for all architectures) of 10^{-3} . Results are averaged over 3 independent runs.

Results. The results are shown in Figure 2, where we report the number of parameters required to reach 99% training accuracy (left plot). Overall, PathCond reaches target accuracy up to $1.5\times$ faster at the same learning rate, and as a side effect also improves parameter efficiency: a 2.5M parameter model matches the performance of 3.25M parameter baseline models. The improvement magnitude varies with the depth. The 3-hidden-layer network (2M parameters) exhibits the strongest gains: training accuracy converges faster with PathCond initialization and the training loss decreases more rapidly toward zero. Deeper networks show more modest but consistent advantages. Notably, ENorm does not yield improvements in this experiment, whereas only PathCond achieves speedups.

Additional learning rates are reported in Appendix K. PathCond matches or exceeds baseline performance across small to moderate learning rates, with the greatest improvements observed at small values where initialization most critically influences training dynamics. As the learning rate increases, the effect becomes less pronounced, yet remains comparable to the baseline and ENorm.

5.2. Generalization

While our method is designed to improve training loss convergence, it does not explicitly target generalization. In this experiment, we show that PathCond accelerates training without degrading generalization performance.

Training Setup. We evaluate our method on the CIFAR-10 fully convolutional architecture (Gitman & Ginsburg, 2017). The architecture processes CIFAR-10 images with channel-wise normalization. The original training set is split into 40,000 images for training and 10,000 for validation. Training is performed for 128 epochs using SGD with a learning rate of 0.001. Weights are initialized using Kaiming’s initialization scheme. We employ a BatchNorm layer after the final fully connected layer for all methods (Baseline, ENorm, and PathCond). Additional learning rates are reported in Appendix L.

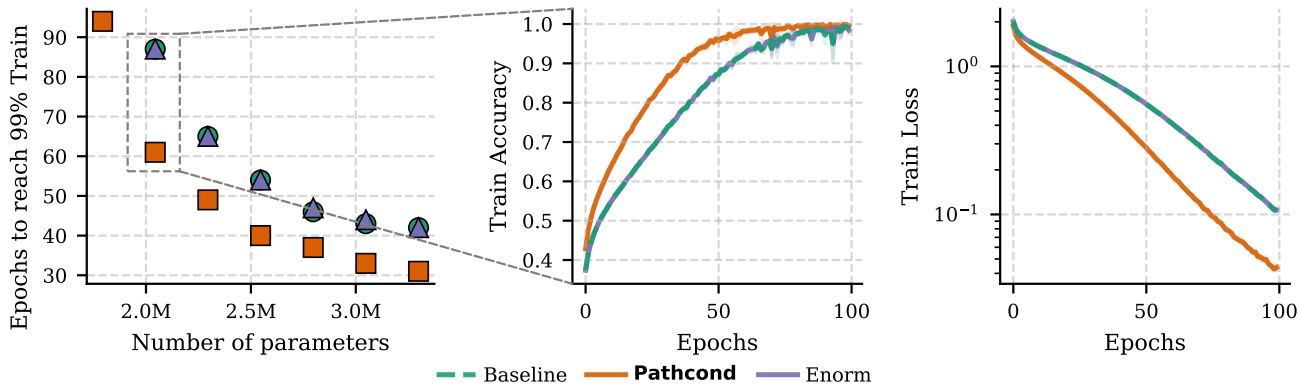


Figure 2. PathCond performance comparison across network depths on CIFAR-10 with multilayer perceptrons (Left) Number of epochs required to reach 99% training accuracy for networks with 2 to 8 hidden layers (abscissa = number of parameters, which increases with depth). (Middle) Training accuracy curves for the 3-hidden-layer network. (Right) Corresponding training loss curves

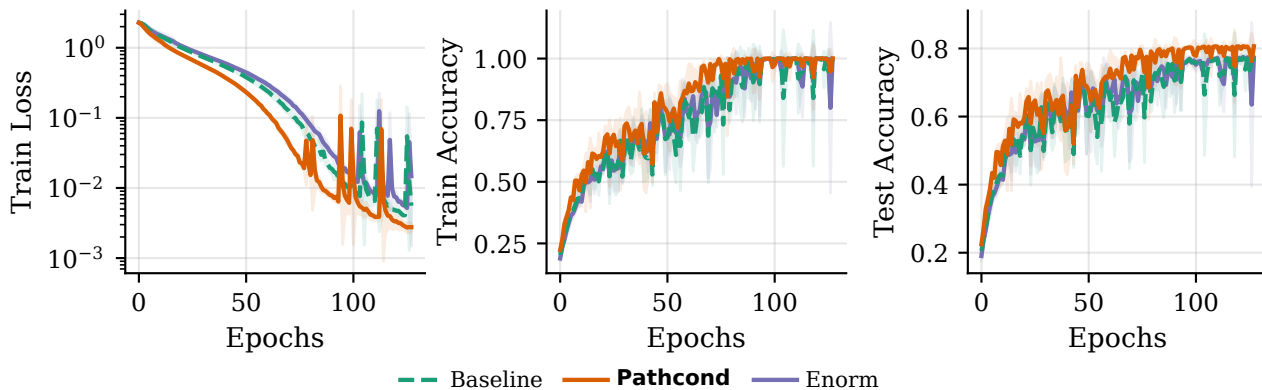


Figure 3. Training dynamics on CIFAR-10 with fully convolutional architecture (CIFAR-NV). (Left) Training loss, (Middle) training accuracy, and (Right) test accuracy.

Results. Figure 3 shows the training dynamics with the fully convolutional architecture. PathCond achieves faster convergence in both training loss (left panel) and training accuracy (middle panel), reaching near-optimal performance approximately 20 epochs earlier than baseline methods. Critically, this acceleration translates to improved test accuracy (right panel): PathCond reaches 80% best test accuracy while Baseline and ENORM plateau at 77%, demonstrating that the improved training dynamics could also enhance rather than compromise generalization.

5.3. What are the Favorable Regimes for PathCond ?

As observed in Figure 2, network architecture influences the effectiveness of our algorithm. This raises a natural question: are there architectures or initializations for which G is already close to the identity (according to the Bregman divergence) without rescaling θ ? Understanding such cases helps identify when PathCond provides the greatest benefits. A simple example is when the diagonal of G is

constant, i.e., where $\exists \alpha > 0$ such that $g = \alpha \mathbf{1}$. In this case, the objective function (9) admits $u = 0$ as its unique minimizer. Consequently, the rescaling matrix is the identity and the algorithm has no effect (proof in Appendix J).

Identifying favorable regimes. Our goal is to identify regimes in which the diagonal exhibits a *wide spread*, i.e., deviates significantly from being constant, by analyzing how g depends on the network architecture and initialization. We hypothesize—and verify empirically—that significant spread in the diagonal correlates with the effectiveness of our rescaling algorithm.

For layered fully-connected ReLU networks (LFCNs) without biases, the expected diagonal coefficients at initialization can be computed explicitly from the network widths n_0, \dots, n_L and the variance of the initialization of each layer σ_k^2 . Standard initializations such as Kaiming (He et al., 2015) have the property that $n_k \sigma_k^2$ is constant across all layers. We denote this value by $a := n_k \sigma_k^2$. We have:

biases are dealt with in Section J.2

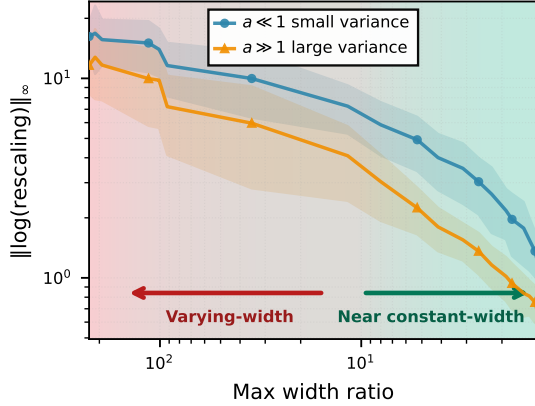


Figure 4. Analysis of the relationship between architectural balance (controlled by the maximum width ratio $\max \frac{n_i}{n_j}$) and log-rescaling magnitude for small and large variance regimes.

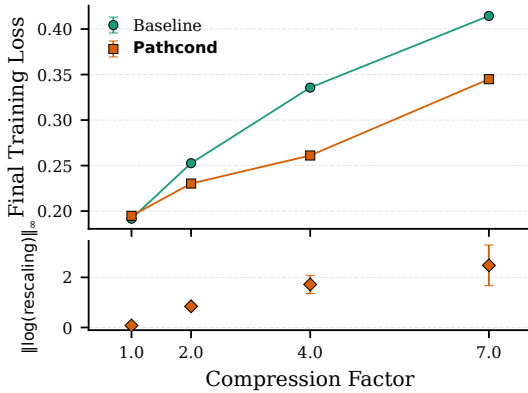


Figure 5. Effect of compression on MNIST autoencoder training. (Top) Final training loss for different compression factors. (Bottom) Maximum absolute value of the log rescaling at initialization.

Proposition 5.1 (Expected diagonal under standard initialization). *For any edge parameter i at layer $k \in \{0, \dots, L-1\}$, the expected i th coefficient of $\text{diag}(G)$ is given by*

$$\mathbb{E}[G_{ii}] = \frac{n_L}{n_{k+1}} a^{L-1} + \frac{n_L}{n_{k+1}} \sum_{j=0}^{k-1} \frac{a^{L-1-j}}{n_j}. \quad (10)$$

The full derivation, including the case with biases, is provided in Appendix J. This result helps us identify regimes in which $\text{diag}(G)$ is close to constant. Consider networks with constant width across layers $n_0 = \dots = n_L := n$:

- **Case $a = 1$:** (94) simplifies to $\mathbb{E}[G_{ii}] = 1 + \frac{k}{n}$. When $n \gg L$, we have $\frac{k}{n} \ll 1$ and thus $\mathbb{E}[G_{ii}] \approx 1$.
- **Case $a \rightarrow +\infty$:** We have $\mathbb{E}[G_{ii}] \sim a^{L-1}(1 + 1/n)$ for $1 \leq k \leq L-1$. Again, for n large enough, $\text{diag}(G)$ is close to $\alpha \mathbf{1}$ with $\alpha = a^{L-1}$.

In contrast, when $a \rightarrow 0$, for all weights on layer k , we have $\mathbb{E}[G_{ii}] \sim \frac{1}{n} a^{L-k}$. Because a is small, there is a large difference in the expected values of g for coefficients on different layers, creating significant spread. In Appendix J.4, we analyze networks with non-constant widths and show that g depends on the width ratios between layers. Based on this analysis, we identify two most favorable regimes:

1. **Varying width architectures:** When layer widths vary significantly ($n_i \neq n_j$), the diagonal exhibits widespread regardless of initialization scale a .
2. **Small variance initialization:** As shown above, for near constant-width architectures ($n_i \approx n$ for all i), the diagonal exhibits significant spread when the initialization standard deviation σ_k is small relative to $1/\sqrt{n}$, i.e., when $a \ll 1$.

In both cases, the diagonal magnitudes vary widely across parameters, creating favorable conditions for PathCond.

Empirical validation. To validate these predictions, we generate networks with fixed depth (8 layers) and mean width (32 neurons per layer), varying the architectural regularity via a Dirichlet-based sampling method (detailed in Appendix J) from nearly uniform (all layers ≈ 32 neurons) to highly non-uniform configurations. For each network, we compute: (1) the width ratio $\max_i n_i / \min_i n_i$, quantifying architectural non-uniformity, and (2) the infinity norm of the log-rescaling factors $\|\log(\text{rescaling})\|_\infty$, measuring the magnitude of required rescaling adjustments. We test both small and large variance initializations. Figure 4 shows a strong correlation between width ratio and log-rescaling magnitude, as well as between small variance initialization and larger rescaling effects, confirming our theoretical predictions.

Experiment on the MNIST Autoencoder. To further validate our characterization of favorable regimes, we consider an autoencoder task where we can systematically vary architectural balance through the compression factor. We follow the experimental setup of Desjardins et al. (2015). The encoder is a fully connected ReLU network with architecture $[784, 784/c_f, 784/c_f^2]$ where the compression factor $c_f \in \{1, 2, 4, 7\}$ (the decoder is symmetric). All weights are initialized using Kaiming uniform initialization. We train for 500 epochs using SGD with a batch size of 128 and learning rate 10^{-3} (additional results in Section M). Each experiment is repeated over 3 independent runs.

Results. Figure 5 shows the final training loss as a function of the compression factor. The effect of PathCond is more pronounced for larger compression factors, which produce more unbalanced architectures, consistent with our theoretical predictions. In all cases, PathCond achieves smaller training loss at convergence.

6. Conclusion

PathCond is a rescaling strategy based on geometric principles and on the path-lifting that aims to accelerate the training of ReLU networks. Our criterion is motivated by the idea that promoting a better-conditioned gradient flow in the network’s lifted space provides a principled approach for minimizing the training loss. This work opens several promising directions: adapting the method for adaptive optimizers with momentum such as Adam and investigating applications to modern architectures including transformers with self-attention mechanisms.

Acknowledgements

This project was supported by the SHARP project of the PEPR-IA (ANR-23-PEIA-0008, granted by France 2030). We thank the Blaise Pascal Center for its computational support, using the SIDUS solution (Quemener & Corvellec, 2013). All experiments were implemented in Python using PyTorch (Paszke et al., 2019) and NumPy (Harris et al., 2020).

References

- Amari, S.-I. Natural gradient works efficiently in learning. *Neural computation*, 10(2):251–276, 1998.
- Armenta, M., Judge, T., Painchaud, N., Skandarani, Y., Lemaire, C., Gibeau Sanchez, G., Spino, P., and Jodoin, P.-M. Neural teleportation. *Mathematics*, 11(2):480, 2023.
- Arora, S., Du, S., Hu, W., Li, Z., and Wang, R. Fine-grained analysis of optimization and generalization for overparameterized two-layer neural networks. In *International conference on Machine Learning (ICML)*, pp. 322–332. PMLR, 2019.
- Azulay, S., Moroshko, E., Nacson, M. S., Woodworth, B. E., Srebro, N., Globerson, A., and Soudry, D. On the implicit bias of initialization shape: Beyond infinitesimal mirror descent. In *International Conference on Machine Learning (ICML)*, volume 139. PMLR, 2021.
- Badrinarayanan, V., Mishra, B., and Cipolla, R. Symmetry-invariant optimization in deep networks. *arXiv preprint arXiv:1511.01754*, 2015.
- Bock, A. A. and Andersen, M. S. Connecting kaporin’s condition number and the bregman log determinant divergence, 2025.
- Bona-Pellissier, J., Malgouyres, F., and Bachoc, F. Local identifiability of deep relu neural networks: the theory. volume 35, 2022.
- Bowman, B. A brief introduction to the neural tangent kernel. 2023.
- Chizat, L., Oyallon, E., and Bach, F. On lazy training in differentiable programming. volume 32, 2019.
- Cormen, T. H., Leiserson, C. E., Rivest, R. L., and Stein, C. *Introduction to algorithms*. MIT press, 2022.
- Desjardins, G., Simonyan, K., Pascanu, R., et al. Natural neural networks. In *Advances in Neural Information Processing Systems (NeurIPS)*, volume 28, 2015.
- Dhillon, I. S. The log-determinant divergence and its applications. In *Householder Symposium XVII, Zeuthen, Germany*, 2008.
- Dinh, L., Pascanu, R., Bengio, S., and Bengio, Y. Sharp minima can generalize for deep nets. In *International Conference on Machine Learning (ICML)*. PMLR, 2017.
- Dominé, C. C. J., Anguita, N., Proca, A. M., Braun, L., Kunin, D., Mediano, P. A. M., and Saxe, A. M. From lazy to rich: Exact learning dynamics in deep linear networks. In *International Conference on Learning Representations (ICLR)*, 2025.
- Dosovitskiy, A., Beyer, L., Kolesnikov, A., Weissenborn, D., Zhai, X., Unterthiner, T., Dehghani, M., Minderer, M., Heigold, G., Gelly, S., Uszkoreit, J., and Houlsby, N. An image is worth 16x16 words: Transformers for image recognition at scale. In *International Conference on Learning Representations (ICLR)*, 2021.
- Du, S. S., Hu, W., and Lee, J. D. Algorithmic regularization in learning deep homogeneous models: Layers are automatically balanced. In *Advances in Neural Information Processing Systems (NeurIPS)*, volume 31, 2018.
- Gao, B. and Pavel, L. On the properties of the softmax function with application in game theory and reinforcement learning. *arXiv preprint arXiv:1704.00805*, 2017.
- Gebhart, T., Saxena, U., and Schrater, P. A unified paths perspective for pruning at initialization. *arXiv preprint arXiv:2101.10552*, 2021.
- Gitman, I. and Ginsburg, B. Comparison of batch normalization and weight normalization algorithms for the large-scale image classification. *arXiv preprint arXiv:1709.08145*, 2017.
- Glorot, X. and Bengio, Y. Understanding the difficulty of training deep feedforward neural networks. In *Proceedings of the thirteenth international conference on artificial intelligence and statistics*, pp. 249–256. JMLR Workshop and Conference Proceedings, 2010.

- Gonon, A. *Harnessing symmetries for modern deep learning challenges: a path-lifting perspective*. PhD thesis, Ecole normale supérieure de lyon-ENS LYON, 2024.
- Gonon, A., Brisebarre, N., Riccietti, E., and Gribonval, R. A path-norm toolkit for modern networks: consequences, promises and challenges. *arXiv preprint arXiv:2310.01225*, 2023.
- Gunasekar, S., Lee, J., Soudry, D., and Srebro, N. Characterizing implicit bias in terms of optimization geometry. In *International Conference on Machine Learning (ICML)*. PMLR, 2018.
- Harris, C. R. et al. Array programming with NumPy. *Nature*, 585:357–362, 2020.
- He, K., Zhang, X., Ren, S., and Sun, J. Delving deep into rectifiers: Surpassing human-level performance on imagenet classification. In *Proceedings of the IEEE international conference on computer vision*, pp. 1026–1034, 2015.
- He, K., Zhang, X., Ren, S., and Sun, J. Deep residual learning for image recognition. In *Proceedings of the IEEE conference on computer vision and pattern recognition*, pp. 770–778, 2016.
- Howard, A. G., Zhu, M., Chen, B., Kalenichenko, D., Wang, W., Weyand, T., Andreetto, M., and Adam, H. Mobilenets: Efficient convolutional neural networks for mobile vision applications. *arXiv preprint arXiv:1704.04861*, 2017.
- Jacot, A., Gabriel, F., and Hongler, C. Neural tangent kernel: Convergence and generalization in neural networks. In *Advances in Neural Information Processing Systems (NeurIPS)*, volume 31, 2018.
- James, W., Stein, C., et al. Estimation with quadratic loss. In *Proceedings of the fourth Berkeley symposium on mathematical statistics and probability*, volume 1, pp. 361–379. University of California Press, 1961.
- Krizhevsky, A., Sutskever, I., and Hinton, G. E. Imagenet classification with deep convolutional neural networks. In *Advances in Neural Information Processing Systems (NeurIPS)*, volume 25, 2012.
- Kulis, B., Sustik, M. A., and Dhillon, I. S. Low-rank kernel learning with bregman matrix divergences. *Journal of Machine Learning Research (JMLR)*, 10(2), 2009.
- Kunin, D., Sagastuy-Brena, J., Ganguli, S., Yamins, D. L., and Tanaka, H. Neural mechanics: Symmetry and broken conservation laws in deep learning dynamics. In *International Conference on Learning Representations (ICLR)*, 2021.
- Kunin, D., Raventós, A., Dominé, C., Chen, F., Klindt, D., Saxe, A., and Ganguli, S. Get rich quick: exact solutions reveal how unbalanced initializations promote rapid feature learning. In *Advances in Neural Information Processing Systems (NeurIPS)*, volume 37, 2024.
- Marcotte, S., Gribonval, R., and Peyré, G. Abide by the law and follow the flow: Conservation laws for gradient flows. In *Advances in Neural Information Processing Systems (NeurIPS)*, volume 36, 2023.
- Marcotte, S., Peyré, G., and Gribonval, R. Intrinsic training dynamics of deep neural networks. *arXiv preprint arXiv:2508.07370*, 2025.
- Martens, J. New insights and perspectives on the natural gradient method. *Journal of Machine Learning Research (JMLR)*, 21(146):1–76, 2020.
- Meng, Q., Zheng, S., Zhang, H., Chen, W., Ma, Z.-M., and Liu, T.-Y. G-SGD: Optimizing reLU neural networks in its positively scale-invariant space. In *International Conference on Learning Representations (ICLR)*, 2019.
- Mustafa, N. and Burkholz, R. Dynamic rescaling for training GNNs. In *Advances in Neural Information Processing Systems (NeurIPS)*, 2024.
- Neyshabur, B., Salakhutdinov, R. R., and Srebro, N. Pathsgd: Path-normalized optimization in deep neural networks. volume 28, 2015.
- Paszke, A., Gross, S., Massa, F., Lerer, A., Bradbury, J., Chanan, G., Killeen, T., Lin, Z., Gimelshein, N., Antiga, L., et al. Pytorch: An imperative style, high-performance deep learning library. In *Advances in Neural Information Processing Systems*, volume 32. 2019.
- Patil, S. M. and Dvornik, C. Phew: Constructing sparse networks that learn fast and generalize well without training data. In *International Conference on Machine Learning (ICML)*, pp. 8432–8442. PMLR, 2021.
- Quemener, E. and Corvellec, M. Sidus—the solution for extreme deduplication of an operating system. *Linux Journal*, 2013(235):3, 2013.
- Sastry, G., Heim, L., Belfield, H., Anderljung, M., Brundage, M., Hazell, J., O’keefe, C., Hadfield, G. K., Ngo, R., Pilz, K., et al. Computing power and the governance of artificial intelligence. *arXiv preprint arXiv:2402.08797*, 2024.
- Saul, L. K. Weight-balancing fixes and flows for deep learning. *Transactions on Machine Learning Research (TMLR)*, 2023a.

- Saul, L. K. Weight-balancing fixes and flows for deep learning. *Transactions on Machine Learning Research (TMLR)*, 2023b. ISSN 2835-8856.
- Silver, D., Huang, A., Maddison, C. J., Guez, A., Sifre, L., Van Den Driessche, G., Schrittwieser, J., Antonoglou, I., Panneershelvam, V., Lanctot, M., et al. Mastering the game of go with deep neural networks and tree search. *Nature*, 529(7587):484–489, 2016.
- Simonyan, K. and Zisserman, A. Very deep convolutional networks for large-scale image recognition. *arXiv preprint arXiv:1409.1556*, 2014.
- Stock, P. and Gribonval, R. An embedding of relu networks and an analysis of their identifiability. *Constructive Approximation*, 57(2):853–899, 2023.
- Stock, P., Graham, B., Gribonval, R., and Jégou, H. Equinormalization of neural networks, 2019.
- Szegedy, C., Liu, W., Jia, Y., Sermanet, P., Reed, S., Anguelov, D., Erhan, D., Vanhoucke, V., and Rabinovich, A. Going deeper with convolutions. In *Proceedings of the IEEE conference on computer vision and pattern recognition*, pp. 1–9, 2015.
- Verbockhaven, M., Rudkiewicz, T., Chevallier, S., and Charpiat, G. Growing tiny networks: Spotting expressivity bottlenecks and fixing them optimally. *Transactions on Machine Learning Research (TMLR)*, 2024. ISSN 2835-8856.
- Von Neumann, J. Thermodynamik quantenmechanischer gesamtheiten. *Nachrichten von der Gesellschaft der Wissenschaften zu Göttingen, Mathematisch-Physikalische Klasse*, 1927:273–291, 1927.
- Zhao, B., Dehmamy, N., Walters, R., and Yu, R. Symmetry teleportation for accelerated optimization. volume 35, 2022.
- Zhao, B., Ganey, I., Walters, R., Yu, R., and Dehmamy, N. Symmetries, flat minima, and the conserved quantities of gradient flow. In *International Conference on Learning Representations (ICLR)*, 2023.

A. Properties of the path-lifting

We have the following properties on the path-lifting

Lemma A.1. *Let $D \in \mathcal{D}$, $\partial\Phi(D\theta) = \partial\Phi(\theta)D^{-1}$.*

Proof. Using the definition of the path-lifting, $\Phi(\theta) := (\Phi_p(\theta))_p$ with $\Phi_p(\theta) := \prod_{i \in \mathcal{P}} \theta_i$, we have

$$\frac{\partial\Phi_p(\theta)}{\partial\theta_i} = \begin{cases} \prod_{\substack{k \in \mathcal{P} \\ k \neq i}} \theta_k & \text{if } p \ni i \\ 0 & \text{otherwise.} \end{cases} \quad (11)$$

Given any $D \in \mathcal{D}$, we have for all $\theta \in \mathbb{R}^p$, $\Phi(D\theta) = \Phi(\theta)$ (Gonon, 2024, Theorem 2.4.1). This means the functions $\theta \mapsto \Phi(\theta)$ and $\theta \mapsto \Phi(D\theta)$ are identical and they share the same Jacobian. Applying the chain rule yields

$$\partial\Phi(\theta) = \partial\Phi(D\theta)D \quad (12)$$

The conclusion follows by multiplying on the right by D^{-1} , which exists by Theorem D.3. \square

B. Gradient in Φ -space

As described in the main text, if $\theta(t)$ follows the gradient flow $\dot{\theta} = \nabla L(\theta)$ of (1) then $z(t) := \Phi(\theta(t))$ satisfies $\dot{z} = \partial_t \Phi(\theta) = -P_\theta \nabla_{\Phi} \ell(\Phi(\theta))$ with $P_\theta = \partial\Phi(\theta) \partial\Phi(\theta)^\top$. As an alternative to the proposed PathCond approach to “align” $P_\theta \nabla_{\Phi} \ell(\Phi(\theta))$ with $\nabla_{\Phi} \ell(\Phi(\theta))$, one could envision a “natural gradient” version along the following route (Amari, 1998; Verboekhaven et al., 2024). Considering any $p \times p$ pre-conditioning matrix $M(\theta)$, it is possible to replace (1) with

$$\dot{\theta} = -M(\theta) \nabla L(\theta). \quad (13)$$

With the same reasoning based on chain rules, if the trajectory $\theta(t)$ is governed by such an ODE then $z(t)$ satisfies the modified ODE

$$\dot{z} = -\partial\Phi(\theta) \dot{\theta} = -\partial\Phi(\theta) M(\theta) \nabla L(\theta) = -\partial\Phi(\theta) M(\theta) \partial\Phi(\theta)^\top \nabla_{\Phi} \ell(\Phi(\theta)). \quad (14)$$

The best alignment with $\nabla_{\Phi} \ell(\Phi(\theta))$ is achieved with the pseudo-inverse $M(\theta) := [\partial\Phi(\theta)^\top \partial\Phi(\theta)]^+$, leading to

$$\dot{z} = -Q_\theta \nabla_{\Phi} \ell(\Phi(\theta)). \quad (15)$$

with Q_θ the $q \times q$ matrix projecting orthogonally onto $\text{range}(\partial\Phi(\theta))$. While this approach leads to the maximum alignment, it involves the computation of the pseudo-inverse of a large $p \times p$ matrix, which is a strong computational bottleneck that PathCond circumvents.

C. Equivalence between different rescaling criteria on toy examples

First example. Consider a minimal architecture with two weights $\theta = (u, v)$, $f_\theta(x) := uvx$, and a loss $L(\theta) = \ell(\Phi(\theta))$ where $\Phi(\theta) := uv$. Straightforward calculus yields

$$\begin{aligned} \nabla\Phi(\theta) &= \begin{pmatrix} v \\ u \end{pmatrix} = \begin{pmatrix} 0 & 1 \\ 1 & 0 \end{pmatrix} \theta \quad \text{and} \quad \nabla^2\Phi(\theta) = \begin{pmatrix} 0 & 1 \\ 1 & 0 \end{pmatrix} \\ \nabla L(\theta) &= \ell'(\Phi(\theta)) \cdot \nabla\Phi(\theta) \\ \nabla^2 L(\theta) &= \underbrace{\ell''(\Phi(\theta)) \cdot \nabla\Phi(\theta) (\nabla\Phi(\theta))^\top}_{=:a} + \underbrace{\ell'(\Phi(\theta)) \cdot \nabla^2\Phi(\theta)}_{=:b} \\ &= a \begin{pmatrix} v^2 & uv \\ uv & u^2 \end{pmatrix} + b \begin{pmatrix} 0 & 1 \\ 1 & 0 \end{pmatrix} = \begin{pmatrix} av^2 & a\Phi(\theta) + b \\ a\Phi(\theta) + b & au^2 \end{pmatrix} \end{aligned}$$

Since Φ is rescaling invariant it follows that for any norm $\|\cdot\|$

$$\arg \min_{\theta' \sim \theta} \|\nabla L(\theta)\| = \arg \min_{\theta' \sim \theta} \|\nabla\Phi(\theta)\| = \arg \min_{\theta' \sim \theta} \|\theta\| \quad (16)$$

and for the special case of the Euclidean norm

$$\arg \min_{\theta' \sim \theta} \text{tr}(\nabla L(\theta)) = \arg \min_{\theta' \sim \theta} \|\theta\|_2. \quad (17)$$

We now turn to the behavior of the condition number $\kappa(\nabla^2 L(\theta))$ and the operator norm $\|\nabla^2 L(\theta)\|_{2 \rightarrow 2}$ by considering the spectrum of $\nabla^2 L(\theta)$, which is made of two eigenvalues $\lambda_- \leq \lambda_+$ such that

$$\begin{aligned} \lambda_+ \lambda_- &= \det(\nabla^2 L(\theta)) = a^2(uv)^2 - (a\Phi(\theta) + b)^2 \\ &= (a\Phi(\theta))^2 - (a\Phi(\theta) + b)^2 = -b(2a\Phi(\theta) + b) =: c \\ \lambda_+ + \lambda_- &= \text{tr}(\nabla^2 L(\theta)) = a(u^2 + v^2) = a\|\theta\|_2^2. \end{aligned}$$

Assuming that $a \geq 0$ (this is the case for example when ℓ is the quadratic loss), the sum $\lambda_+ + \lambda_-$ is thus non-negative, hence $\lambda_+ \geq |\lambda_-|$ and therefore $\|\nabla^2 L(\theta)\|_{2 \rightarrow 2} = \lambda_+$. We also obtain that $\kappa(\nabla^2 L(\theta)) = \lambda_+ / |\lambda_-|$. Notice that each of these quantities can be expressed as $g(\lambda_+, |\lambda_-|)$ where g increases with its first argument, and decreases with its second one. We now investigate how they vary with $\|\theta'\|_2^2$ when $\theta' \sim \theta$.

Since a, b, c can be expressed as a function of $\Phi(\theta)$, they are unchanged if we replace θ by a rescaling equivalent parameter $\theta' \sim \theta$. When varying such a θ' , an increase in $\|\theta'\|_2^2$ increases the sum $\lambda_+ + \lambda_-$ while leaving the product $\lambda_+ \lambda_-$ constant. Let us distinguish two cases:

- case $c \geq 0$: both eigenvalues have the same sign, and since their sum $a\|\theta'\|_2^2$ is positive, they are both positive. Straightforward calculus shows that increasing their sum while keeping their product constant increases the largest one λ_+ while decreasing the smallest one $\lambda_- = |\lambda_-|$. Therefore with g as above the value $g(\lambda_+, \lambda_-)$ increases with $\|\theta'\|_2^2$
- case $c < 0$ here since we have seen that λ_+ remains positive we must have $\lambda_- = -|\lambda_-|$. The same type of reasoning shows that we reach the same conclusion.

Overall it follows that

$$\arg \min_{\theta' \sim \theta} \kappa(\nabla L(\theta)) = \arg \min_{\theta' \sim \theta} \|\nabla L(\theta)\|_{2 \rightarrow 2} = \arg \min_{\theta' \sim \theta} \|\theta\|_2. \quad (18)$$

Second example. The above example is a particular case of a deeper toy example where $\theta = (u_1, \dots, u_L)$ and $\Phi(\theta) = u_1 \dots u_L$. Similar computations (we skip the details) show that when all entries u_i are nonzero, denoting $\theta^{-1} := (u_i^{-1})_{i=1}^L$

$$\begin{aligned} \nabla \Phi(\theta) &= (\Phi(\theta)/u_i)_{i=1}^L = \Phi(\theta) \cdot \theta^{-1} \\ \nabla L(\theta) &= \ell'(\Phi(\theta)) \cdot \nabla \Phi(\theta) = \underbrace{\ell'(\Phi(\theta)) \cdot \Phi(\theta)}_{=: a(\Phi(\theta))} \cdot \theta^{-1} \\ \nabla^2 L(\theta) &= a(\Phi(\theta)) \cdot \text{offdiag}(\theta^{-1}(\theta^{-1})^\top) + (\Phi(\theta))^2 \ell''(\Phi(\theta)) \cdot \theta^{-1}(\theta^{-1})^\top \end{aligned}$$

We deduce that $\text{tr}(\nabla^2 L(\theta)) = (\Phi(\theta))^2 \ell''(\Phi(\theta)) \|\theta^{-1}\|_2^2$. Overall we obtain with the same reasoning that

$$\arg \min_{\theta' \sim \theta} \|\nabla L(\theta)\| = \arg \min_{\theta' \sim \theta} \text{tr}(\nabla^2 L(\theta)) = \arg \min_{\theta' \sim \theta} \|\theta^{-1}\|_2. \quad (19)$$

D. Characterization of the rescaling symmetry

Let $\mathcal{G} = (V, E)$ be a fixed directed acyclic graph (DAG), representing a fixed network architecture, with vertices V called neurons and edges E . For a neuron $v \in V$, we define the sets of antecedents and successors as

$$\text{ant}(v) := \{u \in V \mid (u, v) \in E\}, \quad \text{suc}(v) := \{u \in V \mid (v, u) \in E\}. \quad (20)$$

Neurons with no antecedents (resp. no successors) are called *input* (resp. *output*) neurons, and their sets are denoted $N_{\text{in}} := \{v \in V \mid \text{ant}(v) = \emptyset\}$ and $N_{\text{out}} := \{v \in V \mid \text{suc}(v) = \emptyset\}$ respectively. The input and output dimensions are $d_{\text{in}} := |N_{\text{in}}|$ and $d_{\text{out}} := |N_{\text{out}}|$. Neurons in $\mathcal{H} := V \setminus (N_{\text{in}} \cup N_{\text{out}})$ are called *hidden neurons*, and we denote their cardinality

by $H := |\mathcal{H}|$. Note that for any hidden neuron $v \in \mathcal{H}$, we have $\text{ant}(v) \neq \emptyset$ and $\text{suc}(v) \neq \emptyset$, i.e., there exist both incoming and outgoing edges (Gonon, 2024, Definition 2.2.2).

To parametrize this graph in the context of neural networks, we perform a topological ordering (Cormen et al., 2022) and assign indices to all neurons and edges. All parameters (weights along edges and biases on neurons) can then be arranged into a vector $\theta \in \mathbb{R}^p$, where p is the total number of parameters. As the architecture is fixed, this vector fully represents our network.

Definition D.1 (Neuron-wise rescaling symmetry). Let $v \in \mathcal{H}$ be a hidden neuron and $\lambda > 0$ a scaling factor. We define the sets of incoming and outgoing parameter indices associated to v as

$$\text{in}_v := \{\text{index}(b_v)\} \cup \{\text{index}(\theta_{u \rightarrow v}) \mid u \in \text{ant}(v)\} \quad (21)$$

and

$$\text{out}_v := \{\text{index}(\theta_{v \rightarrow u}) \mid u \in \text{suc}(v)\}, \quad (22)$$

where b_v denotes the bias of neuron v , and $\theta_{u \rightarrow v}$ (resp. $\theta_{v \rightarrow u}$) denotes the weight of edge $(u, v) \in E$ (resp. $(v, u) \in E$) (Gonon, 2024, Definition 2.2.2). The diagonal matrix $D_{\lambda, v} \in \mathbb{R}^{p \times p}$ associated to the *neuron-wise rescaling symmetry* (Stock & Gribonval, 2023, Def. 2.3) is defined by its diagonal entries:

$$(D_{\lambda, v})_{ii} = \begin{cases} \lambda & \text{if } i \in \text{in}_v \\ 1/\lambda & \text{if } i \in \text{out}_v \\ 1 & \text{otherwise.} \end{cases} \quad (23)$$

This matrix implements a rescaling of neuron v by factor λ : incoming weights and bias are multiplied by λ , while outgoing weights are divided by λ .

We can then define the following set:

Definition D.2 (Rescaling symmetry group). We denote by \mathcal{D} the subgroup generated by the neuron-wise rescaling symmetries (Stock & Gribonval, 2023, Def. 2.3):

$$\mathcal{D} = \text{gr}(\{D_{\lambda, v} \mid v \in \mathcal{H}, \lambda \in \mathbb{R}_*^+\}). \quad (24)$$

Lemma D.3. *The rescaling symmetry group admits the following explicit characterization:*

$$\mathcal{D} = \left\{ \prod_{v \in \mathcal{H}} D_{\lambda_v, v} \mid \lambda \in (\mathbb{R}_*^+)^H \right\}. \quad (25)$$

The order of the product does not matter since diagonal matrices commute.

Proof. Let $A := \{\prod_{v \in \mathcal{H}} D_{\lambda_v, v} \mid \lambda \in (\mathbb{R}_*^+)^H\}$. Since diagonal matrices commute and $D_{\lambda, v}^{-1} = D_{1/\lambda, v}$, it is straightforward to show that A is stable under product and inversion, and is therefore a subgroup of the group of strictly positive diagonal matrices. Let us show that it contains all $D_{\lambda, v}$. Indeed, given any $v \in \mathcal{H}$ and $\lambda > 0$, choosing $\lambda_v = \lambda$ and $\lambda_{v'} = 1$ for all $v' \in \mathcal{H} \setminus \{v\}$ yields $\prod_{v' \in \mathcal{H}} D_{\lambda_{v'}, v'} = D_{\lambda, v}$. By minimality of the generated subgroup, we therefore have $\mathcal{D} \subset A$. Conversely, every element of A is a product of elements of \mathcal{D} , hence an element of \mathcal{D} by the group property. \square

For the next definitions, we recall some notation from Gonon et al. (2023).

Definition D.4 (Path in a DAG). (Gonon et al., 2023, Definition A.1) A path of a DAG $\mathcal{G} = (V, E)$ is any sequence of neurons v_0, \dots, v_d such that each $v_i \rightarrow v_{i+1}$ is an edge. Such a path is denoted $p = v_0 \rightarrow \dots \rightarrow v_d$. The length of a path $p = v_0 \rightarrow \dots \rightarrow v_d$ is $\text{length}(p) = d$ (the number of edges).

Definition D.5 (Path lifting). (Gonon et al., 2023, Definition A.2) For a path $p \in \mathcal{P}$ with $p = v_0 \rightarrow \dots \rightarrow v_d$, the path lifting is defined as

$$\Phi_p(\theta) := \begin{cases} \prod_{\ell=1}^{\text{length}(p)} \theta_{v_{\ell-1} \rightarrow v_\ell} & \text{if } v_0 \in N_{\text{in}}, \\ b_{v_0} \prod_{\ell=1}^{\text{length}(p)} \theta_{v_{\ell-1} \rightarrow v_\ell} & \text{otherwise,} \end{cases} \quad (26)$$

where an empty product equals 1 by convention. The path-lifting $\Phi(\boldsymbol{\theta})$ of $\boldsymbol{\theta}$ over the entire graph is

$$\Phi(\boldsymbol{\theta}) := (\Phi_p(\boldsymbol{\theta}))_{p \in \mathcal{P}}. \quad (27)$$

By a slight abuse of notation, we extend the path-lifting to diagonal matrices by applying it to their diagonal entries. For $D \in \mathbb{R}^{p \times p}$ diagonal, we define

$$\Phi(D) := \Phi((D_{ii})_{i=1, \dots, p}). \quad (28)$$

Definition D.6 (Admissible rescaling matrices). We denote by $\Phi^{-1}(\mathbf{1})^+$ the set of diagonal matrices with strictly positive entries whose path-lifting equals the all-ones vector:

$$\Phi^{-1}(\mathbf{1})^+ := \{D \in \mathbb{R}^{p \times p} \text{ diagonal} \mid \Phi(D) = \mathbf{1} \text{ and } D_{ii} > 0 \text{ for all } i\}. \quad (29)$$

Lemma D.7. *The set of admissible rescaling matrices coincides with $\Phi^{-1}(\mathbf{1})^+$:*

$$\mathcal{D} = \Phi^{-1}(\mathbf{1})^+. \quad (30)$$

Proof. We prove both inclusions.

- $\mathcal{D} \subseteq \Phi^{-1}(\mathbf{1})^+$

Let $D \in \mathcal{D}$. By Theorem D.3, there exists $\boldsymbol{\lambda} \in (\mathbb{R}_*^+)^{\mathcal{H}}$ such that

$$D = \prod_{v \in \mathcal{H}} D_{\lambda_v, v}. \quad (31)$$

Since $\boldsymbol{\lambda} \in (\mathbb{R}_*^+)^{\mathcal{H}}$, we have $D_{ii} > 0$ for all i .

It remains to show that $\Phi(D) = \mathbf{1}$. By Gonon (2024, Theorem 2.4.1), the rescaling symmetry property ensures that for any $\boldsymbol{\theta} \in \mathbb{R}^p$,

$$\Phi(D\boldsymbol{\theta}) = \Phi(\boldsymbol{\theta}), \quad (32)$$

Applying this property with $\boldsymbol{\theta} = \mathbf{1}$, we obtain

$$\Phi(D\mathbf{1}) = \Phi(\mathbf{1}) = \mathbf{1}, \quad (33)$$

where the last equality holds because $\Phi_p(\mathbf{1}) = \prod_{i \in \mathcal{P}} 1 = 1$ for all paths $p \in \mathcal{P}$.

Now, observe that $(D\mathbf{1})_i = D_{ii}$ for all i . Therefore,

$$\Phi(D) = \Phi(D\mathbf{1}) = \mathbf{1}. \quad (34)$$

This shows that $D \in \Phi^{-1}(\mathbf{1})^+$, hence $\mathcal{D} \subseteq \Phi^{-1}(\mathbf{1})^+$.

- $\Phi^{-1}(\mathbf{1})^+ \subseteq \mathcal{D}$

Let $D \in \Phi^{-1}(\mathbf{1})^+$. We can write $D = \text{diag}(\mathbf{d})$ for some $\mathbf{d} \in (\mathbb{R}_*^+)^p$.

We want to show that $D \in \mathcal{D}$, which by Theorem D.3 means showing that D can be written as a product of neuron-wise rescaling matrices:

$$D = \prod_{v \in \mathcal{H}} D_{\lambda_v, v} \quad (35)$$

for some $\boldsymbol{\lambda} \in (\mathbb{R}_*^+)^{\mathcal{H}}$.

Notation. To simplify the exposition, for any neuron $v \in V$ and edge $(u, v) \in E$, we denote:

$$d_v := d_{\text{index}(b_v)} \quad \text{and} \quad d_{u \rightarrow v} := d_{\text{index}(\theta_{u \rightarrow v})}, \quad (36)$$

i.e., d_v is the rescaling factor of the bias of neuron v , and $d_{u \rightarrow v}$ is the rescaling factor of the weight on edge (u, v) .

Characterization of \mathcal{D} . Recall from Theorem D.1 that the matrix $D_{\lambda_v, v}$ multiplies the bias and all incoming weights of neuron v by λ_v , while dividing all outgoing weights by λ_v . Therefore, a diagonal matrix D belongs to \mathcal{D} if and only if there exist rescaling factors $\lambda_v > 0$ for each $v \in \mathcal{H}$ such that:

(i) For each hidden neuron $v \in \mathcal{H}$, the bias rescaling factor satisfies:

$$d_v = \lambda_v. \quad (37)$$

(ii) For each edge $(u, v) \in E$, the weight rescaling factor satisfies:

$$d_{u \rightarrow v} = \frac{\lambda_v}{\lambda_u}, \quad (38)$$

where we adopt the convention $\lambda_u = 1$ for $u \in N_{\text{in}}$ and $\lambda_v = 1$ for $v \in N_{\text{out}}$.

Indeed, condition (i) ensures that each bias is rescaled by the appropriate factor, while condition (ii) captures the combined effect on edges: as an outgoing edge from u , the weight is divided by λ_u ; as an incoming edge to v , it is multiplied by λ_v .

Proof strategy. Given $D \in \Phi^{-1}(\mathbf{1})^+$, we define for all hidden neurons $v \in \mathcal{H}$:

$$\lambda_v := d_v > 0. \quad (39)$$

This definition automatically satisfies condition (i). To show that $D \in \mathcal{D}$, it therefore suffices to verify condition (ii), namely that for any edge $(u, v) \in E$:

$$d_{u \rightarrow v} = \frac{\lambda_v}{\lambda_u}. \quad (40)$$

We distinguish three cases based on the nature of the neurons u and v . Note that we do not need to consider the case where $u \in N_{\text{in}}$ and $v \in N_{\text{out}}$ simultaneously, as such edges would bypass all hidden neurons and involve no rescaling from \mathcal{D} .

Case 1: $v \in N_{\text{out}}$

Consider the path $p = (u \rightarrow v)$. By hypothesis, $\Phi(D) = \mathbf{1}$, so

$$\Phi_p(D) = d_u \cdot d_{u \rightarrow v} = 1. \quad (41)$$

Since $d_u = \lambda_u$, we obtain

$$d_{u \rightarrow v} = \frac{1}{\lambda_u} \quad (42)$$

Case 2: $u \in N_{\text{in}}$

Consider a path p starting from input neuron u and passing through the edge (u, v) . We can write $p = (u \rightarrow v \rightarrow w_1 \rightarrow \dots \rightarrow w_k)$ where $w_k \in N_{\text{out}}$. Consider also the path $p' = (v \rightarrow w_1 \rightarrow \dots \rightarrow w_k)$ which coincides with p after vertex v . By hypothesis, $\Phi(D) = \mathbf{1}$, we have

$$\Phi_p(D) = d_{u \rightarrow v} \prod_{\ell=1}^k d_{w_{\ell-1} \rightarrow w_\ell} = 1, \quad (43)$$

where $w_0 := v$, and

$$\Phi_{p'}(D) = d_v \prod_{\ell=1}^k d_{w_{\ell-1} \rightarrow w_\ell} = 1. \quad (44)$$

Dividing the first equation by the second yields

$$d_{u \rightarrow v} = d_v = \lambda_v. \quad (45)$$

Case 3: $u, v \in \mathcal{H}$

Let $(u, v) \in E$ be an edge between two hidden neurons.

Consider any path p starting from neuron u and passing through the edge (u, v) . We can write $p = (u \rightarrow v \rightarrow w_1 \rightarrow \dots \rightarrow w_k)$ where $w_k \in N_{\text{out}}$. Consider also the path $p' = (v \rightarrow w_1 \rightarrow \dots \rightarrow w_k)$ which coincides with p after vertex v . Since both u and v are hidden neurons, both paths start from their respective biases. By hypothesis, $\Phi(D) = \mathbf{1}$, we have

$$\Phi_p(D) = d_u \cdot d_{u \rightarrow v} \prod_{\ell=1}^k d_{w_{\ell-1} \rightarrow w_\ell} = 1, \quad (46)$$

where $w_0 := v$, and

$$\Phi_{p'}(D) = d_v \prod_{\ell=1}^k d_{w_{\ell-1} \rightarrow w_\ell} = 1. \quad (47)$$

Dividing the first equation by the second yields

$$d_u \cdot d_{u \rightarrow v} = d_v. \quad (48)$$

Since $d_v = \lambda_v$ and $d_u = \lambda_u$, we obtain

$$d_{u \rightarrow v} = \frac{\lambda_v}{\lambda_u}. \quad (49)$$

In all cases, equation (40) holds, which shows that $D = \prod_{v \in \mathcal{H}} D_{\lambda_v, v} \in \mathcal{D}$. Therefore, $\Phi^{-1}(\mathbf{1})^+ \subseteq \mathcal{D}$. □

E. Bregman matrix divergences

We first formally introduce Bregman matrix divergences. Let S^q be the space of $q \times q$ symmetric matrices on \mathbb{R} . Given a strictly convex and differentiable function $\zeta : S^q \rightarrow \mathbb{R}$, the Bregman divergence between matrices X and Y is defined as

$$d_\zeta(X||Y) = \zeta(X) - \zeta(Y) - \text{tr}(\nabla \zeta(Y)^\top (X - Y)). \quad (50)$$

The most well-known example is built from the squared Frobenius norm $\zeta(X) = \|X\|_F^2$, which yields $d_\zeta(X||Y) = \|X - Y\|_F^2$. The logdet divergence corresponds to $\zeta(X) = -\log \det(X)$ (James et al., 1961), and the von Neumann divergence to $\zeta(X) = \text{tr}(X \log X - X)$ (Von Neumann, 1927). Within the class of Bregman matrix divergences, *spectral divergences* are particularly important: they take the form $\zeta(X) = \varphi \circ \lambda(X)$, where λ denotes the vector of eigenvalues of X in decreasing order and φ is a strictly convex real-valued function on vectors (Kulis et al., 2009). The aforementioned examples are all spectral divergences: $\varphi(x) = \sum_i |x_i|^2$ for the Frobenius norm, $\varphi(x) = -\sum_i \log(x_i)$ for the logdet divergence, and $\varphi(x) = \sum_i (x_i \log x_i - x_i)$ for the von Neumann divergence.

Spectral divergences with $\varphi(x) = \sum_i \psi(x_i)$ for some $\psi : \mathbb{R} \rightarrow \mathbb{R}$ admit the expression (Kulis et al., 2009, Lemma 1) s

$$d_\zeta(X||Y) = \sum_{ij} (u_i^\top v_j)^2 (\psi(\lambda_i(X)) - \psi(\lambda_j(Y)) - (\lambda_i(X) - \lambda_j(Y)) \nabla \psi(\lambda_j(Y))), \quad (51)$$

where u_i (resp. v_j) is an eigenvector associated to the i -th largest eigenvalue $\lambda_i(X)$ of X (resp. Y). Hence, $d_\zeta(X||Y)$ can be written as $d_\zeta(X||Y) = \sum_{ij} (u_i^\top v_j)^2 \text{div}_\psi(\lambda_i(X)||\lambda_j(Y))$ where div_ψ is the Bregman divergence associated to ψ .

Definition E.1. Consider $\zeta = \varphi \circ \lambda$ with $\varphi(x) = \sum_i \psi(x_i)$ that induces a spectral divergence as described above. We define the ζ^+ divergence as the divergence *that only considers the nonzero eigenvalues of the matrices*. In other words,

$$d_{\zeta^+}(X||Y) := \sum_{\substack{i:\lambda_i(X) \neq 0 \\ j:\lambda_j(Y) \neq 0}} (u_i^\top v_j)^2 \text{div}_\psi(\lambda_i(X)||\lambda_j(Y)). \quad (52)$$

We have the following lemma.

Lemma E.2. Consider a spectral divergence on S^q with $\zeta(X) = \varphi \circ \lambda(X)$ where φ can be written as $\varphi(x) = \sum_i \psi(x_i)$ for some strictly convex and differentiable function $\psi : \mathbb{R} \rightarrow \mathbb{R}$ and ζ^+ as defined in (52). Then, for any $A \in \mathbb{R}^{q \times p}$

$$d_{\zeta^+}(AA^\top || I_q) = d_{\zeta^+}(A^\top A || I_p). \quad (53)$$

Proof. When $Y = I_q$, $d_{\zeta^+}(X||Y)$ becomes $\sum_{i:\lambda_i(X) \neq 0} \|u_i\|_2^2 \text{div}_\psi(\lambda_i(X)||1) = \sum_{i:\lambda_i(X) \neq 0} \text{div}_\psi(\lambda_i(X)||1)$ thus only depends on the eigenvalues of X . Using that the nonzero eigenvalues of AA^\top and $A^\top A$ are the same concludes. \square

Now we apply this result to the logdet divergence and we have

Lemma E.3. Take $\zeta(X) = -\log \det(X)$. Then, for any $A \in \mathbb{R}^{q \times p}$,

$$\begin{aligned} d_{\zeta^+}(AA^\top || I_q) &= \text{tr}(A^\top A) - \sum_{i:\lambda_i(A^\top A) \neq 0} \log \lambda_i(A^\top A) - \text{rank}(A) \\ &= \text{tr}(A^\top A) - \log \det_+(A^\top A) - \text{rank}(A), \end{aligned} \quad (54)$$

where $\det_+(X)$ is the generalized determinant, that is the product of the nonzeros eigenvalues of X .

Proof. Based on the proof of Equation (52) we have $d_{\zeta^+}(AA^\top || I_q) = \sum_{i:\lambda_i(A^\top A) \neq 0} \text{div}_\psi(\lambda_i(A^\top A)||1)$ where $\psi = -\log$. So in this case $\text{div}_\psi(x||y) = -\log(x) + \log(y) + \frac{1}{y}(x-y) = -\log(\frac{x}{y}) + \frac{x}{y} - 1$. Using this formula, $\text{rank}(A^\top A) = \text{rank}(A)$ and $\sum_{i:\lambda_i(A^\top A) \neq 0} \lambda_i(A^\top A) = \text{tr}(A^\top A)$ gives the result. \square

F. PathCond optimization problem

We detail here the definition of the PathCond optimization problem. We recall that $P_\theta = \partial\Phi(\theta)\partial\Phi(\theta)^\top \in \mathbb{R}^{q \times q}$ is the path-kernel. We define $G = G_\theta = \partial\Phi(\theta)^\top \partial\Phi(\theta) \in \mathbb{R}^{p \times p}$ and consider $\zeta(X) = -\log \det(X)$ and d_ζ, d_{ζ^+} the associated spectral divergence and its version that considers only nonzero eigenvalues, see Definition E.1. Furthermore, we place ourselves in the regime $q \geq p$ (which is the case for most DAG ReLU networks, except very small ones).

Proposition F.1. Denote $r = \text{rank}(\partial\Phi(\theta))$ and let $\partial\Phi(\theta) = U\Sigma V^\top$ be a compact SVD decomposition of $\partial\Phi(\theta)$, i.e., $U \in \mathbb{R}^{q \times r}, V \in \mathbb{R}^{p \times r}, U^\top U = V^\top V = I_r, \Sigma = \text{diag}(\sigma_1, \dots, \sigma_r) > 0$. For any admissible $D = \text{diag}(d_1, \dots, d_p) \in \mathcal{D}$ and $\alpha > 0$, we have

$$d_{\zeta^+}(\alpha P_{D\theta} || I_q) = d_{\zeta^+}(\alpha G_{D\theta} || I_p) = \alpha \sum_{i=1}^p d_i^{-2} G_{ii} - r \log(\alpha) - \log \det(\Sigma^2) - \log \det(V^\top D^{-2} V) - r. \quad (55)$$

When $r = p$, the matrix $G_{D\theta}$ is positive definite for any $D \in \mathcal{D}$ and

$$d_{\zeta^+}(\alpha P_{D\theta} || I_q) = d_{\zeta^+}(\alpha G_{D\theta} || I_p) = d_\zeta(\alpha G_{D\theta} || I_p). \quad (56)$$

Moreover, the minimization over $\alpha > 0, D \in \mathcal{D}$ of these quantities is equivalent to the problem

$$\min_{D' \in \mathcal{D}} p \log \left(\sum_{i=1}^p d'_i G_{ii} \right) - \sum_{i=1}^p \log(d'_i). \quad (57)$$

Precisely if D' solves (57) then $D := D'^{-1/2}$ and $\alpha = \frac{p}{\sum_i d_i^{-2} G_{ii}}$ minimize the previous quantities.

Proof. First we recall that \det_+ is the product of the nonzero eigenvalues. First, we have from Lemma A.1 $\partial\Phi(D\theta) = \partial\Phi(\theta)D^{-1}$. Using this property, Lemma E.3 with $A = \sqrt{\alpha}\partial\Phi(\theta)D^{-1}$, and the commutation property of the trace, we have

$$\begin{aligned} d_{\zeta^+}(\alpha P_{D\theta} || I_q) &= d_{\zeta^+}(\alpha \partial\Phi(\theta)D^{-1}(\partial\Phi(\theta)D^{-1})^\top || I_q) \\ &= d_{\zeta^+}(AA^\top || I_q) \\ &= \text{tr}(A^\top A) - \log \det_+(A^\top A) - \text{rank}(A) \\ &= \alpha \text{tr}(D^{-2}G) - r \log(\alpha) - \log \det_+(D^{-1}GD^{-1}) - r. \end{aligned} \quad (58)$$

Using the compact singular value decomposition of $\partial\Phi(\theta)$ we have that $D^{-1}GD^{-1} = D^{-1}V\Sigma^2V^\top D^{-1}$. Since V has orthogonal columns and D is invertible, the nonzero eigenvalues of $D^{-1}V\Sigma^2V^\top D^{-1}$ are the same as the nonzero eigenvalues of $\Sigma^2V^\top D^{-2}V$. Indeed, if λ is such an eigenvalue then $D^{-1}V\Sigma^2V^\top D^{-1}x = \lambda x \implies V\Sigma^2V^\top D^{-1}x = \lambda Dx$. Thus $Dx \in \text{Im}(V)$ and there is y such that $Dx = Vy$ that is $x = D^{-1}Vy$. Thus, $V\Sigma^2V^\top D^{-1}D^{-1}Vy =$

$\lambda DD^{-1}Vy$ that is $V\Sigma^2V^\top D^{-2}Vy = \lambda Vy$, left multiplying by V^\top gives that λ is an eigenvalue of $\Sigma^2V^\top D^{-2}V$. The converse is straightforward.

Using the definition of \det_+ we get that

$$\det_+(D^{-1}GD^{-1}) = \det_+(\Sigma^2V^\top D^{-2}V) = \det(\Sigma^2V^\top D^{-2}V) = \det(\Sigma^2) \det(V^\top D^{-2}V), \quad (59)$$

where we used that $\Sigma^2(V^\top D^{-2}V)$ is invertible since both Σ and $V^\top D^{-2}V$ are invertible (the latter is positive definite because $D > 0$). This gives the first formula (55). Consequently, for any diagonal matrix D we have

$$\min_{\alpha > 0} d_{\zeta+}(\alpha P_{D\theta} || I_q) = -r \log(r) + r \log\left(\sum_{i=1}^p d_i^{-2} G_{ii}\right) - \log \det(\Sigma^2) - \log \det(V^\top D^{-2}V), \quad (60)$$

as the first order conditions for the loss in α give $\alpha = \frac{r}{\sum_i d_i^{-2} G_{ii}}$ (the $G_{ii} \geq 0$ since the matrix is positive semi-definite).

When $r = p$, G is full rank and since $G_{D\theta} = D^{-1}GD^{-1}$ it follows that $G_{D\theta}$ is positive definite hence $d_{\zeta+}(\alpha G_{D\theta} || I_p) = d_{\zeta}(\alpha G_{D\theta} || I_p)$ for any $\alpha > 0$ and any diagonal matrix D . In this case, since V is square and unitary, $\log \det(V^\top D^{-2}V) = \log \det(D^{-2}) + \log \det(VV^\top) = \log \det(D^{-2})$. In light of (60), the minimization over $\alpha > 0$ and $D \in \mathcal{D}$ of $d_{\zeta+}(\alpha P_{D\theta} || I_q)$ thus corresponds to choosing $\alpha = \frac{r}{\sum_i d_i^{-2} G_{ii}}$ where $D \in \mathcal{D}$ minimizes the sum of terms that depend on D in (60): $r \log \sum_{i=1}^p d_i^{-2} G_{ii} - \log \det(D^{-2})$. This corresponds to (57) with the change of variable $D' = D^{-2}$ (observe that $D' \in \mathcal{D}$ if, and only if, $D \in \mathcal{D}$) and the expression of the determinant of a diagonal matrix. \square

Remark F.2. With the same reasoning, when $r = \text{rank}(\partial\Phi(\theta)) < p$ the minimization of (55) over α, D is equivalent to

$$\min_{D' \in \mathcal{D}} r \log\left(\sum_{i=1}^p d'_i G_{ii}\right) - \log \det(V^\top D' V). \quad (61)$$

We now prove that the optimization problem (57) can be rewritten as (9) and that it has a solution.

Lemma F.3. Consider $B \in \mathbb{R}^{p \times H}$ with entries in $\{1, -1, 0\}$ indicating whether a parameter enters (-1), leaves (1), or is unrelated to (0) a given neuron. Precisely, $B = (b_1, \dots, b_H)$ with

$$\forall \text{ neuron } h, (b_h)_i = \begin{cases} -1 & \text{if } i \in \text{in}_v \\ 1 & \text{if } i \in \text{out}_v \\ 0 & \text{otherwise.} \end{cases} \quad (62)$$

Then $\mathcal{D} = \{\text{diag}(\exp(Bu)), u \in \mathbb{R}^H\}$. Thus (57) is equivalent to

$$\min_{u \in \mathbb{R}^H} F(u) \quad \text{with } F(u) := p \log\left(\sum_{i=1}^p e^{(Bu)_i} G_{ii}\right) - \sum_{i=1}^p (Bu)_i, \quad (63)$$

in the sense that if u solves (63) then $D' := \text{diag}(\exp(Bu))$ solves (57).

Proof. Let $D' \in \mathcal{D}$, and d be the vector of \mathbb{R}^p such that $D' = \text{diag}(d)$. We want to show that d can be written as $d = \exp(Bu)$. Thanks to Theorem D.3, we know that there exists $\lambda \in (\mathbb{R}^{+*})^H$ such that

$$d = \bigodot_{v \in \mathcal{H}} d_{\lambda_v, v} \quad (64)$$

Where \bigodot denotes the Hadamard coordinate wise product and $d_{\lambda_v, v}$ is the diagonal of the neuron-wise rescaling matrix $D_{\lambda_v, v}$ introduced in Theorem D.1. For $v \in \mathcal{H}$, $\lambda_v \in \mathbb{R}^{+*}$, by definition, we get

$$(d_{\lambda_v, v})_i = \begin{cases} \lambda_v & \text{if } i \in \text{in}_v \\ 1/\lambda_v & \text{if } i \in \text{out}_v \\ 1 & \text{otherwise.} \end{cases} \quad (65)$$

But because $\lambda_v \in \mathbb{R}^{+*}$, there exists an $u_v \in \mathbb{R}$ such that $\lambda_v = \exp(-u_v)$. We can rewrite $d_{\lambda_v, v}$ as

$$(d_{\lambda_v, v})_i = \begin{cases} \exp(-u_v) & \text{if } i \in \text{in}_v \\ \exp(u_v) & \text{if } i \in \text{out}_v \\ \exp(0) & \text{otherwise.} \end{cases} \quad (66)$$

We can rewrite the previous equation with a column of B , precisely:

$$d_{\lambda_v, v} = \exp(u_v b_v) \quad (67)$$

where the \exp is taken coordinate-wise. Now let i an integer with $1 \leq i \leq p$, thanks to (64), we get

$$d_i = \prod_{h=1}^H (d_{\lambda_h, h})_i = \prod_{h=1}^H \exp(u_h b_h)_i = \prod_{h=1}^H \exp(B_{ih} u_h) \quad (68)$$

So,

$$d_i = \exp\left(\sum_{h=1}^H B_{ih} u_h\right) \quad (69)$$

We can conclude that

$$d = \exp(Bu) \quad (70)$$

Vice-versa, if d writes this way it is a Hadamard product of $d_h := \exp(b_h u_h)$, so that $D' = \text{diag}(d)$ is a product of diagonal matrices which can easily be checked to belong to \mathcal{D} . We conclude using that \mathcal{D} is a group. \square

To prove existence of a solution we will use the following result.

Lemma F.4. *If $G_{ii} > 0$ for each i and $B \neq 0$ satisfies $1 \notin \text{span}(B)$, then the function F in (63) is coercive.*

Proof. F can be written as $F(u) = f(Bu)$ where $f(x) = p \log(\sum_{i=1}^p e^{x_i} G_{ii}) - \sum_i x_i$. We have that $\sum_{i=1}^p e^{x_i} G_{ii} \geq \max_{k \in \llbracket p \rrbracket} e^{x_k} G_{kk}$ thus $f(x) \geq p \max_{k \in \llbracket p \rrbracket} \{x_k + \log(G_{kk})\} - \sum_i x_i \geq pc + \sum_i (\max_k x_k - x_i)$ where $c = \min_k \log(G_{kk}) > -\infty$ using the hypothesis on G . Denoting e_i the i -th standard basis vector, this gives

$$F(u) \geq pc + \sum_{i=1}^n \left(\max_k \{ \langle e_k^\top, Bu \rangle \} - \langle e_i^\top, Bu \rangle \right). \quad (71)$$

We define

$$\forall u, \alpha(u) = \sum_{i=1}^p \left(\max_k \{ \langle e_k^\top, Bu \rangle \} - \langle e_i^\top, Bu \rangle \right). \quad (72)$$

Clearly for any $t \geq 0$, $\alpha(t \cdot u) = t \cdot \alpha(u)$. To conclude that the function is coercive we introduce

$$\beta := \min_{\|u\|_2=1} \alpha(u). \quad (73)$$

Since α is continuous, this minimum is attained. Also, for any $u \neq 0$,

$$F(u) = F\left(\|u\|_2 \cdot \frac{u}{\|u\|_2}\right) \geq pc + \alpha\left(\|u\|_2 \cdot \frac{u}{\|u\|_2}\right) = pc + \|u\|_2 \cdot \alpha\left(\frac{u}{\|u\|_2}\right) \geq pc + \beta \|u\|_2. \quad (74)$$

Proving that $\beta > 0$ is thus sufficient to ensure the coercivity of F . For this, first note that for any $u, i \in \llbracket p \rrbracket$,

$$\max_k \{ \langle e_k^\top, Bu \rangle \} - \langle e_i^\top, Bu \rangle \geq 0, \quad (75)$$

hence $\beta \geq 0$, and we only need to rule out the case $\beta = 0$. The above inequality indeed also shows $\beta = 0$ if and only if there exists u such that $\forall i, \max_k \{ \langle e_k^\top, Bu \rangle \} = \langle e_i^\top, Bu \rangle$. This condition is equivalent to the existence of u such that $\langle e_i^\top, Bu \rangle = \text{cte}, \forall i$, that is to say the existence of u such that $Bu = \text{cte}$, which is not possible since $1 \notin \text{span}(B)$. \square

To conclude we use the second lemma

Lemma F.5. *Consider B as defined in (62). Then $1 \notin \text{span}(B)$.*

Proof. By contradiction, assume that $1 \in \text{span}(B)$ then there is u such that $Bu = 1$, and by Theorem F.3 the diagonal matrix $D := \text{diag}(\exp(Bu)) = e^1 I$ belongs to \mathcal{D} and thanks to Theorem D.7 it belongs to $\Phi^{-1}(\mathbf{1})^+$. However for any path $p \in P$, $\Phi_p(e^1 I) = \prod_{i \in p} e^1 \neq 1$ which leads to the desired contradiction. We conclude that $1 \notin \text{span}(B)$. \square

Corollary F.6. *Suppose that $\forall i, G_{ii} > 0$. The optimization problem (9) always has a solution.*

Proof. Since the logsumexp function is convex (Gao & Pavel, 2017, Lemma 4), one easily shows that the function F is convex. It is also continuous, and coercive by Theorem F.4 and Theorem F.5. So there exists a minimizer. \square

Finally we prove that (9) can be solved via simple alternating minimization, where each minimization admits a closed form.

Lemma F.7. *We note $\rho_{i,h} = e^{(Bu)_i - B_{ih}u_h}$. If $g > 0$, for any neuron h , the problem $\min_{u_h \in \mathbb{R}} F(u_1, \dots, u_h, \dots, u_H)$ has a solution given by $\log(r_h)$ where r_h is the unique positive root of the polynomial $B(A+p)X^2 + ADX + C(A-p)$ with*

$$\begin{aligned} A &:= |\{i \in \text{in}_h\}| - |\{i \in \text{out}_h\}|, \quad \mathcal{B} := \sum_{i \in \text{out}_h} \rho_{i,h} g_i \\ \mathcal{C} &:= \sum_{i \in \text{in}_h} \rho_{i,h} g_i, \quad \mathcal{D} := \sum_{i \in \text{other}_h} \rho_{i,h} g_i. \end{aligned}$$

Proof. We note, $g_i = G_{ii}$, $f(x) = p \log(\sum_i e^{x_i} g_i) - \sum_i x_i$ such that $F(u) = f(Bu)$. We have first

$$\nabla f(x) = \frac{p}{\langle e^x \odot g, \mathbf{1} \rangle} (e^x \odot g) - \mathbf{1}. \quad (76)$$

Since $\nabla F(u) = B^\top \nabla f(Bu)$ the h -th coordinate of this gradient is

$$\begin{aligned} (\nabla F(u))_h &= \langle b_h, \nabla f(Bu) \rangle = \frac{p}{\langle e^{Bu} \odot g, \mathbf{1} \rangle} \langle b_h, e^{Bu} \odot g \rangle - \langle b_h, \mathbf{1} \rangle \\ &= p \frac{\sum_{i \in \text{out}_h} e^{(Bu)_i} g_i - \sum_{i \in \text{in}_h} e^{(Bu)_i} g_i}{\sum_i e^{(Bu)_i} g_i} + \left(\sum_{i \in \text{in}_h} 1 - \sum_{i \in \text{out}_h} 1 \right). \end{aligned} \quad (77)$$

Now writing $u = (u_1, \dots, u_h, \dots, u_H)$ and using that

$$(Bu)_i = \sum_k B_{ik} u_k = B_{ih} u_h + \sum_{k \neq h} B_{ik} u_k, \quad (78)$$

and with the notation $\rho_{i,h} := \exp((Bu)_i - B_{ih}u_h)$, we get

$$e^{(Bu)_i} = \rho_{i,h} e^{B_{ih}u_h} = \begin{cases} \rho_{i,h} e^{u_h} & i \in \text{out}_h \\ \rho_{i,h} e^{-u_h} & i \in \text{in}_h \\ \rho_{i,h} & i \in \text{other}_h. \end{cases} \quad (79)$$

So with A, B, C, D defined in the lemma, (77) becomes

$$\begin{aligned} (\nabla F(u))_h &= p \frac{\sum_{i \in \text{out}_h} e^{u_h} \rho_{i,h} g_i - \sum_{i \in \text{in}_h} e^{-u_h} \rho_{i,h} g_i}{\sum_{i \in \text{out}_h} e^{u_h} \rho_{i,h} g_i + \sum_{i \in \text{in}_h} e^{-u_h} \rho_{i,h} g_i + \sum_{i \in \text{other}_h} \rho_{i,h} g_i} + A \\ &= p \frac{e^{u_h} \mathcal{B} - e^{-u_h} \mathcal{C}}{e^{u_h} \mathcal{B} + e^{-u_h} \mathcal{C} + \mathcal{D}} + A. \end{aligned} \quad (80)$$

Hence

$$(\nabla F(u))_h = 0 \iff \mathcal{B}(A+p)e^{u_h} + \mathcal{A}\mathcal{D} + \mathcal{C}(A-p)e^{-u_h} = 0. \quad (81)$$

Introducing $X = e^{u_h} > 0$, the problem of finding a minimizer u_h (which we know exists by coercivity of F) reduces to finding a positive root of the polynomial

$$\mathcal{B}(\mathcal{A} + p)X^2 + \mathcal{A}DX + \mathcal{C}(\mathcal{A} - p). \quad (82)$$

One easily checks that $-p < \mathcal{A} < p$ and $\mathcal{B}, \mathcal{C} > 0$ (since $g > 0$), hence $\mathcal{B}(\mathcal{A} + p) > 0, \mathcal{C}(\mathcal{A} - p) < 0$ thus the polynomial has exactly one positive root. \square

G. Computation of the diagonal of G

Proposition G.1. *The diagonal of $G = \partial\Phi^\top \partial\Phi$ can be computed efficiently as:*

$$\text{diag}(G) = \nabla_{\theta^2} \|\Phi(\theta)\|_2^2 \quad (83)$$

where ∇_{θ^2} denotes differentiation with respect to the vector of squared parameters $\theta^2 = (\theta_1^2, \dots, \theta_p^2)$, or equivalently $\theta^2 = \theta \odot \theta$ where \odot denotes the Hadamard (element-wise) product and p is the number of parameters.

Proof. Denote \mathcal{P} the set of all paths. For a parameter i , we have by making the change of variable $\theta_i^2 = \omega_i$:

$$G_{ii} = \sum_{\substack{\mathcal{p} \in \mathcal{P} \\ \mathcal{p} \ni i}} \prod_{\substack{k \in \mathcal{p} \\ k \neq i}} \theta_k^2 \quad (\text{definition of } G_{ii}) \quad (84)$$

$$= \sum_{\substack{\mathcal{p} \in \mathcal{P} \\ \mathcal{p} \ni i}} \prod_{\substack{k \in \mathcal{p} \\ k \neq i}} \omega_k \quad (85)$$

$$= \sum_{\substack{\mathcal{p} \in \mathcal{P} \\ \mathcal{p} \ni i}} \frac{\partial}{\partial \omega_i} \Phi_{\mathcal{p}}(\omega) \quad (\text{Because } \Phi_{\mathcal{p}}(\omega) = \prod_{k \in \mathcal{p}} \omega_k, \text{ the derivative is straightforward}) \quad (86)$$

$$= \frac{\partial}{\partial \omega_i} \sum_{\mathcal{p} \in \mathcal{P}} \Phi_{\mathcal{p}}(\omega) \quad (\text{terms with } i \notin \mathcal{p} \text{ do not depend on } \omega_i \text{ and vanish with the derivative}) \quad (87)$$

$$= (\nabla_{\omega} \|\Phi(\omega)\|_1)_i \quad (\text{Because } \Phi_{\mathcal{p}}(\omega) \geq 0) \quad (88)$$

$$= (\nabla_{\theta^2} \|\Phi(\theta)\|_2^2)_i \quad (\text{Because } \|\Phi_{\mathcal{p}}(\omega)\|_1 = \|\Phi_{\mathcal{p}}(\theta)\|_2^2) \quad (89)$$

\square

H. Detailed Algorithm and Complexity Analysis

Algorithm 3 gives the full pseudocode of `PathCond`. The matrix $B \in \mathbb{R}^{p \times H}$ is never formed explicitly; only its non-zero entries are stored. Since each parameter (edge) appears in at most two columns of B —once as an outgoing edge and once as an incoming edge—we have $\text{nnz}(B) \leq 2p$. The $O(n_{\text{iter}} \cdot p)$ total complexity rests on two incremental updates.

Dual variable $v = Bu$. At each coordinate-descent step, only u_h changes by some increment δ , inducing the update $\Delta v = \delta b_h$, where b_h is the h -th column of B . Since b_h has only $|\text{out}_h| + |\text{in}_h|$ non-zero entries, this costs $O(|\text{out}_h| + |\text{in}_h|)$ rather than $O(p)$.

Global auxiliary sum E . Computing the degree polynomial (Lemma 4.1) requires

$$\mathcal{D} = \sum_{i \in \text{other}_h} e^{v_i} g_i,$$

a sum over $p - |\text{out}_h| - |\text{in}_h| \approx p$ terms. Naïvely evaluating this for each of the H neurons would give $O(pH)$ per sweep. Instead, we maintain the global sum $E = \sum_{i=1}^p e^{v_i} g_i$ and recover

$$\mathcal{D} = E - S_{\text{out}} - S_{\text{in}}, \quad S_{\text{out}} = \sum_{i \in \text{out}_h} e^{v_i} g_i, \quad S_{\text{in}} = \sum_{i \in \text{in}_h} e^{v_i} g_i,$$

at cost $O(|\text{out}_h| + |\text{in}_h|)$. After updating v , the sum E is refreshed within the same budget by recomputing only the affected terms. One full sweep therefore costs $\sum_{h=1}^H O(|\text{out}_h| + |\text{in}_h|) = O(p)$, and the total complexity over n_{iter} sweeps is $O(n_{\text{iter}} \cdot p)$, linear in the number of parameters per iteration.

Algorithm 3 PathCond : Path-conditioned rescaling

Input : DAG ReLU network with parameters θ ; scaling weights $g = \text{diag}(G) \in \mathbb{R}^p$; tolerance $\varepsilon > 0$; maximum iterations n_{iter}

Output : Rescaled parameters $\tilde{\theta} = \text{diag}(e^v) \theta$

```

7  $u \leftarrow \mathbf{0} \in \mathbb{R}^H$ ; // Primal variables
8  $v \leftarrow \mathbf{0} \in \mathbb{R}^p$ ; // Dual variables, invariant:  $v = Bu$ 
9  $E \leftarrow \sum_{i=1}^p g_i$ ; // Global sum  $E = \sum_i e^{v_i} g_i$ , initialized with  $v = 0$ 
10 for  $k = 0, \dots, n_{\text{iter}} - 1$  do
11    $\Delta \leftarrow 0$  for each neuron  $h = 1, \dots, H$  do
12     // Index sets of outgoing/incoming parameters of neuron  $h$ 
13      $\text{out}_h \leftarrow \{i : B_{i,h} = +1\}$   $\text{in}_h \leftarrow \{i : B_{i,h} = -1\}$ 
14     // Recover  $\mathcal{D}$  from global sum in  $O(|\text{out}_h| + |\text{in}_h|)$ 
15      $S_{\text{out}} \leftarrow \sum_{i \in \text{out}_h} e^{v_i} g_i$   $S_{\text{in}} \leftarrow \sum_{i \in \text{in}_h} e^{v_i} g_i$   $\mathcal{D} \leftarrow E - S_{\text{out}} - S_{\text{in}}$ 
16     // Coefficients of the degree polynomial (Lemma 4.1)
17      $\mathcal{A} \leftarrow |\text{in}_h| - |\text{out}_h|$   $\mathcal{B} \leftarrow \sum_{i \in \text{out}_h} e^{v_i - u_h} g_i$ ; //  $\rho_{i,h} = e^{v_i - u_h}$  for  $i \in \text{out}_h$ 
18      $\mathcal{C} \leftarrow \sum_{i \in \text{in}_h} e^{v_i + u_h} g_i$ ; //  $\rho_{i,h} = e^{v_i + u_h}$  for  $i \in \text{in}_h$ 
19     // Optimal step: solve  $\mathcal{B}(\mathcal{A}+p)X^2 + \mathcal{A}\mathcal{D}X + \mathcal{C}(\mathcal{A}-p) = 0$ 
20      $r_h \leftarrow \frac{-\mathcal{A}\mathcal{D} + \sqrt{(\mathcal{A}\mathcal{D})^2 - 4\mathcal{B}(\mathcal{A}+p)\mathcal{C}(\mathcal{A}-p)}}{2\mathcal{B}(\mathcal{A}+p)}$   $\delta \leftarrow \ln r_h - u_h$ ; //  $u_h^{(k+1)} = \ln r_h$ 
21     // Incremental update of  $v$  and  $E$  in  $O(|\text{out}_h| + |\text{in}_h|)$ 
22      $v_i \leftarrow v_i + \delta$  for  $i \in \text{out}_h$   $v_i \leftarrow v_i - \delta$  for  $i \in \text{in}_h$   $E \leftarrow \mathcal{D} + \sum_{i \in \text{out}_h} e^{v_i} g_i + \sum_{i \in \text{in}_h} e^{v_i} g_i$ 
23      $u_h \leftarrow u_h + \delta$   $\Delta \leftarrow \Delta + |\delta|$ 
24   if  $\Delta < \varepsilon$  then break;
25 return  $\tilde{\theta} = \text{diag}(e^v) \theta$ 

```

I. Architecture Statistics: Number of Parameters, Hidden Units, and Paths

This section reports detailed architectural statistics for several standard convolutional neural network (CNN) models commonly used in computer vision. For each architecture, we consider the following three quantities:

- **Parameters:** the total number of trainable parameters (weights and biases) in the network.
- **Hidden Units:** the total number of hidden channels across all convolutional layers, serving as the convolutional analogue of hidden neurons in fully connected networks.
- **Number of Paths:** the total number of distinct computational paths from the input to the output induced by the network architecture.

The number of hidden units is computed by summing the output dimensionality (i.e., the number of channels) of each convolutional layer, excluding the final classification layer.

To compute the number of paths, we rely on the path-norm formalism introduced by [Gonon et al. \(2023\)](#). Let Π denote the set of all paths in the network, and let $\Phi(\theta)$ denote the vector of path products associated with parameters θ . The path-1 norm is defined as

$$\|\Phi(\theta)\|_1 = \sum_{p \in \Pi} |\Phi_p(\theta)|.$$

By setting all network parameters to one, i.e., $\theta = \mathbf{1}$, each path product equals one, and therefore

$$\|\Phi(\mathbf{1})\|_1 = \sum_{p \in \Pi} 1 = |\Pi|,$$

which exactly corresponds to the number of paths in the architecture. Importantly, this quantity can be computed efficiently using a single forward pass through the network [Gonon et al. \(2023\)](#).

[Table 1](#) summarizes these statistics for several widely used CNN architectures.

Model	Parameters	Hidden Units	Paths
ResNet-18 (He et al., 2016)	11,689,512	4,800	1.13×10^{58}
ResNet-34 (He et al., 2016)	21,797,672	8,512	6.68×10^{109}
ResNet-50 (He et al., 2016)	25,557,032	26,560	7.16×10^{140}
AlexNet (Krizhevsky et al., 2012)	61,100,840	9,344	1.21×10^{30}
VGG-16 (Simonyan & Zisserman, 2014)	138,357,544	12,416	1.15×10^{56}
CIFAR-NV (Gitman & Ginsburg, 2017)	2,616,576	1,792	2.46×10^{28}

Table 1. Architectural statistics for common convolutional neural networks.

J. Regimes Analysis at Initialization

We begin with a fundamental observation about the rescaling algorithm.

Proposition J.1 (Trivial case: constant diagonal). *If the diagonal of G is constant, i.e., there exists $\alpha > 0$ such that*

$$g = \alpha \mathbf{1},$$

then the objective of the rescaling problem (9) admits $u = 0$ as its unique minimizer. Consequently, the rescaling matrix is the identity and the algorithm has no effect.

Proof. Let’s go back to (9)

$$F(u) = p \log \left(\sum_{i=1}^p e^{(Bu)_i} G_{ii} \right) - \sum_{i=1}^p (Bu)_i.$$

If $G_{ii} = \alpha > 0$ for all i , then

$$F(u) = p \log \left(\frac{\alpha}{p} \sum_{i=1}^p e^{(Bu)_i} \right) - \sum_{i=1}^p (Bu)_i = p \log \alpha + p \log \left(\frac{1}{p} \sum_{i=1}^p e^{(Bu)_i} \right) - p \left(\frac{1}{p} \sum_{i=1}^p (Bu)_i \right).$$

Because the log is concave on \mathbb{R}_*^+ , by Jensen’s inequality, we have

$$F(u) \geq p \log(\alpha),$$

which is achieved at $u = 0$. Since the objective is strictly convex, $u = 0$ is the unique minimizer. \square

J.1. The Matrix G

Consider a neural network represented as a directed acyclic graph (DAG) with ReLU, identity, and max-pooling operations. Let Φ denote the path-feature map and define the *path-magnitude matrix*

$$G := \partial \Phi^\top \partial \Phi.$$

We focus on its diagonal $g = \text{diag}(G)$, whose entries encode path magnitudes.

For any parameter i (edge weight or bias), the corresponding diagonal entry is

$$g_i = \sum_{\substack{p \in \mathcal{P} \\ p \ni i}} \prod_{\substack{j \in \mathcal{P} \\ j \neq i}} \theta_j^2, \tag{90}$$

where \mathcal{P} denotes the set of all paths ending at an output neuron.

Expected path magnitudes. At initialization, parameters θ_i are independent random variables. By independence, the linearity of expectation yields

$$\mathbb{E}[g_i] = \sum_{\substack{p \in \mathcal{P} \\ p \ni i}} \prod_{\substack{j \in p \\ j \neq i}} \mathbb{E}[\theta_j^2]. \quad (91)$$

J.2. Layered Fully-Connected ReLU Networks

We specialize to layered fully-connected ReLU networks (LFCNs) (Gonon et al., 2023). Such a network is specified by a depth L and widths (n_0, \dots, n_L) , where layer k maps \mathbb{R}^{n_k} to $\mathbb{R}^{n_{k+1}}$.

We distinguish two types of paths: (i) paths starting from input neurons, and (ii) paths starting from bias parameters. As is customary, we omit a bias in the last layer since it does not affect expressivity.

Let $\sigma_k^2 := \mathbb{E}[\theta_j^2]$ for any edge parameter in layer k . This assumption of layer-wise constant variance is standard in neural network initialization schemes such as Xavier/Glorot initialization (Glorot & Bengio, 2010) and He initialization (He et al., 2015), which are designed to maintain activation variance across layers during forward and backward passes.

Counting paths through a parameter. To compute expected path magnitudes via equation (91), we decompose the calculation into: (1) counting paths passing through a parameter, and (2) computing the expected squared magnitude of each path type.

Consider an edge parameter w located in layer k (connecting layer k to layer $k + 1$). The number of paths passing through w and originating from input neurons equals the number of input-to-output paths in the reduced network obtained by fixing layers k and $k + 1$ to a single neuron:

$$N_{\text{edge},k}^{\text{input}} = \prod_{\substack{i=0 \\ i \neq k, k+1}}^L n_i.$$

This counts all combinations of neurons in layers other than k and $k + 1$.

For any such path p containing w , the expected contribution to g_w (excluding w itself) is

$$\mathbb{E} \left[\prod_{\substack{j \in p \\ j \neq w}} \theta_j^2 \right] = \prod_{\substack{\ell=0 \\ \ell \neq k}}^{L-1} \sigma_\ell^2,$$

where the product ranges over all layers except layer k (which contains w) and the output layer L (which has no outgoing edges).

Additionally, we must account for paths originating from bias parameters in layers 0 to $k - 1$. A path starting from a bias in layer $i < k$ and passing through w traverses all layers from $i + 1$ to L , excluding the neurons in layers k and $k + 1$. The number of such paths is

$$N_{\text{edge},k}^{\text{bias},i} = \prod_{\substack{j=i+1 \\ j \neq k, k+1}}^L n_j.$$

Each such path has expected squared magnitude (excluding w from the product)

$$\prod_{\substack{j=i \\ j \neq k}}^{L-1} \sigma_j^2,$$

where the product starts from layer i (containing the bias) and excludes layer k .

For a bias parameter b in layer k , the analysis is simpler. Such a bias only participates in paths from layer k onward to the output. The number of such paths is

$$N_{\text{bias},k} = \prod_{i=k+1}^L n_i,$$

and each path has expected squared magnitude (excluding the bias itself from the product)

$$\prod_{i=k+1}^{L-1} \sigma_i^2.$$

Expected path magnitudes: closed-form formula. Combining path counts with their corresponding expected squared magnitudes yields the following closed-form expression for expected path magnitudes:

$$\mathbb{E}[g_i] = \begin{cases} \prod_{i=k+1}^L n_i \prod_{i=k+1}^{L-1} \sigma_i^2, & \text{if } i \text{ is a bias in layer } k, \\ \prod_{\substack{i=0 \\ i \neq k, k+1}}^L n_i \prod_{\substack{i=0 \\ i \neq k}}^{L-1} \sigma_i^2 + \sum_{i=0}^{k-1} \prod_{\substack{j=i+1 \\ j \neq k, k+1}}^L n_j \prod_{\substack{j=i \\ j \neq k}}^{L-1} \sigma_j^2, & \text{if } i \text{ is an edge in layer } k. \end{cases} \quad (92)$$

Introducing the quantities $a_k := n_k \sigma_k^2$, equation (92) simplifies to:

$$\mathbb{E}[g_i] = \begin{cases} n_L \sigma_{k+1}^2 \prod_{i=k+2}^{L-1} a_i, & \text{if } i \text{ is a bias in layer } k, \\ n_L \sigma_{k+1}^2 \prod_{\substack{i=0 \\ i \neq k, k+1}}^{L-1} a_i + n_L \sigma_{k+1}^2 \sum_{i=0}^{k-1} \sigma_i^2 \prod_{\substack{j=i+1 \\ j \neq k}}^{L-1} a_j, & \text{if } i \text{ is an edge in layer } k. \end{cases} \quad (93)$$

J.3. Classical Initializations

For standard initializations such as He or Kaiming initialization, one has

$$a_k = n_k \sigma_k^2 = a, \quad \forall k,$$

for some constant $a > 0$.

Proposition J.2 (Expected diagonal under standard initialization). *For a LFCN with standard initialization, the expected path magnitude associated with a parameter in layer k is given by*

$$\mathbb{E}[g_i] = \begin{cases} \frac{n_L}{n_{k+1}} a^{L-1-k}, & \text{if } i \text{ is a bias in layer } k, \\ \frac{n_L}{n_{k+1}} a^{L-1} + \frac{n_L}{n_{k+1}} \sum_{i=0}^{k-1} \frac{a^{L-1-i}}{n_i}, & \text{if } i \text{ is an edge in layer } k. \end{cases} \quad (94)$$

J.4. Consequences for the Rescaling Algorithm

For the rescaling algorithm to have a non-trivial effect, the expected diagonal of G must exhibit variation across parameters. The analysis above reveals that this depends delicately on both the network architecture and the initialization scheme.

Architectures with non-constant width. We focus on edge parameters as their behavior already allows to highlight architectural regimes where the expected diagonal of G exhibits significant variations in magnitude. For an edge parameter in layer k , equation (94) becomes

$$\mathbb{E}[g_i] = \frac{n_L}{n_{k+1}} a^{L-1} + \frac{n_L}{n_{k+1}} \sum_{i=0}^{k-1} \frac{a^{L-1-i}}{n_i}.$$

The behavior of this expression depends critically on the regime of the variance scaling factor a .

In the *large variance regime* ($a \rightarrow +\infty$), the first term dominates:

$$\mathbb{E}[g_i] \sim \frac{n_L}{n_{k+1}} a^{L-1}.$$

The expected path magnitude is determined primarily by the ratio n_L/n_{k+1} . The ratio between $\mathbb{E}[g_i]$ and $\mathbb{E}[g_j]$ for parameters in different layers is of order n_k/n_{k+1} , provided that a is large enough.

In the *small variance regime* ($a \rightarrow 0$), the sum dominates and retains only its last term:

$$\mathbb{E}[g_i] \sim \frac{n_L}{n_{k+1}} \frac{a^{L-k}}{n_{k-1}}.$$

This regime exhibits much stronger variation in expected path magnitudes. The ratio between $\mathbb{E}[g_i]$ and $\mathbb{E}[g_j]$ for parameters in different layers can be of order $1/a$, which is very large.

In the *critical case* $a = 1$, corresponding for instance to Kaiming normal initialization with unit gain and fan-in scaling, we obtain

$$\mathbb{E}[g_i] = \frac{n_L}{n_{k+1}} \left(1 + \sum_{i=0}^{k-1} \frac{1}{n_i} \right), \quad k \in \{1, \dots, L-1\}.$$

Hence, unless the width is constant across all layers, the expected diagonal of G exhibits non-trivial variation.

J.5. Constant-Width Networks

Setup. We now consider multi-layer perceptrons with constant width $n_i = n$ for all hidden layers $i \in \{0, \dots, L-1\}$. In this simplified setting, the expected path magnitude for an edge parameter in layer k reduces to:

$$\mathbb{E}[g_i] = \begin{cases} a^{L-1}, & \text{if } k = 0, \\ a^{L-1} + \frac{1}{n} \sum_{i=1}^k a^{L-i}, & \text{if } k \in \{1, \dots, L-1\}. \end{cases} \quad (95)$$

Case $a = 1$. When $a = 1$, equation (95) simplifies to

$$\mathbb{E}[g_i] = 1 + \frac{k}{n}, \quad k \in \{0, \dots, L-2\}. \quad (96)$$

The expected path magnitude increases linearly with depth. For networks with large width $n \gg L$, the diagonal is approximately constant, and the rescaling algorithm has little effect.

Case $a \neq 1$. When $a \neq 1$, the geometric series yields

$$\mathbb{E}[g_i] = a^{L-1} + \frac{a^{L-1}}{n} \cdot \frac{1 - (1/a)^k}{1 - 1/a}, \quad k \in \{0, \dots, L-1\}. \quad (97)$$

Large variance regime: $a \rightarrow +\infty$. In this regime,

$$\mathbb{E}[g_i] \sim \begin{cases} a^{L-1}, & \text{if } k = 0, \\ a^{L-1} (1 + 1/n), & \text{if } k \in \{1, \dots, L-1\}. \end{cases} \quad (98)$$

Small variance regime: $a \rightarrow 0$. In this regime,

$$\mathbb{E}[g_i] \sim \begin{cases} a^{L-1}, & \text{if } k = 0, \\ a^{L-1} (1 + 1/n), & \text{if } k = 1, \\ \frac{a^{L-k}}{n}, & \text{if } k \in \{2, \dots, L-1\}. \end{cases} \quad (99)$$

The diagonal exhibits a multi-level structure with significant variation across layers, especially for deeper layers.

J.6. Summary and Implications

Based on the analysis above, we identify regimes in which the rescaling algorithm is expected to have a non-trivial effect.

- **Varying-width architectures:** For networks with non-uniform layer widths, regardless of the initialization scale a , the expected diagonal of G is non-constant across layers. The rescaling algorithm is expected to have a significant effect on such irregular configurations.
- **Near constant-width architectures with small variance:** For networks with approximately uniform width $n_i \approx n$ for all i , the algorithm has a non-trivial effect when initialized with small variance, i.e., when $a \ll 1$. In this regime, the diagonal exhibits significant variation across layers despite the regularity of the architecture.
- **Near constant-width architectures with critical initialization:** For such regular configurations with $a = 1$, the diagonal varies as $1 + k/n$. The effect is significant when the depth L is comparable to or larger than the width n .
- **Near constant-width architectures with large variance:** For near constant-width networks with $a \gg 1$, the diagonal exhibits a simple two-level structure. The rescaling may help but the effect is limited to distinguishing the first layer from subsequent layers.

Conclusion. The rescaling algorithm is expected to have the most significant impact in two scenarios:

1. Varying-width architectures, regardless of initialization.
2. Near constant-width architectures of width n , initialized with small standard deviation relative to $1/\sqrt{n}$.

In both cases, the expected path magnitudes exhibit significant variation across parameters, leading to ill-conditioning of the path-magnitude matrix G that the rescaling algorithm can address.

We empirically validate these assumptions through a controlled experiment on synthetic networks.

Experimental Setup. We generate multiple networks with a fixed depth of 8 layers and a mean width of 32 neurons per layer, ensuring a total budget of $8 \times 32 = 256$ neurons distributed across all hidden layers. To systematically vary the width regularity of the network architecture, we introduce a concentration parameter $\alpha \in [10^{-1}, 10^2]$ that controls a symmetric Dirichlet distribution used to sample the proportion of neurons allocated to each layer. When α is very large, the Dirichlet distribution becomes highly concentrated around uniform proportions, resulting in near constant-width configurations (all layers ≈ 32 neurons). Conversely, when α is small, the distribution allows for greater variability in the proportions, creating varying-width architectures where some layers are significantly wider or narrower than others. To ensure architectural validity, each layer is guaranteed a minimum width of 1 neuron, with the remaining budget distributed proportionally according to the Dirichlet samples using a largest remainder method to maintain the exact total neuron count.

We repeat this experiment 20 times, sampling 20 different α values in each run to ensure statistical robustness.

Remark. We can notice that these favorable regimes are common in practice. Even when most hidden layers share a near constant-width, input and output dimensions often differ significantly, giving rise to an inherently non-uniform configuration. For instance, in the CIFAR-10 experiments (Figure 2), the 3072-dimensional input and 10-dimensional output create architectural irregularity despite the many intermediate layers of width 500. However, as depth increases, the network approaches near constant-width behavior, which explains why the performance gains decrease for very deep networks.

K. Additional Experiments for Section 5.1

We provide here additional experiments complementing Section 5.1, covering a broader range of learning rates.

Figure 6 demonstrates that PathCond achieves strong performance at small to moderate learning rates, consistent with our theoretical framework where proper initialization critically affects training dynamics. However, performance degrades at larger learning rates, where optimization instabilities overshadow initialization benefits and our theoretical assumptions (small learning rate regime) no longer hold.

Path-conditioned training: a principled way to rescale ReLU neural networks

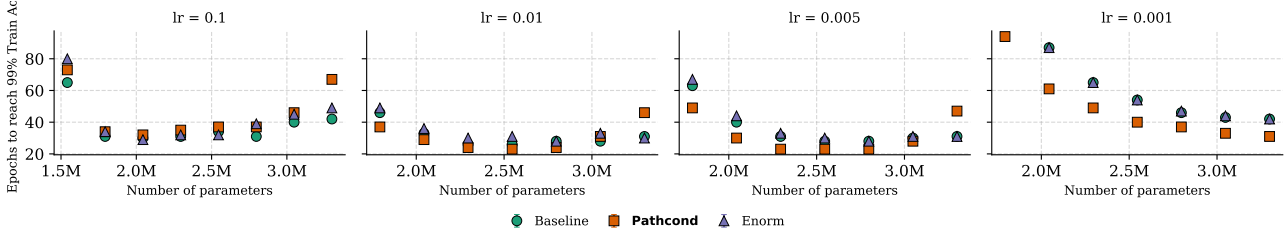


Figure 6. Convergence speed across different learning rates and network sizes.

L. Additional Experiments for Section 5.2

We provide complementary experiments for Section 5.2, exploring the impact of learning rate on the generalization benefits of PathCond across a wider range of values.

Figure 7 presents training and test dynamics for learning rates ranging from 10^{-2} to 10^{-4} . Consistent with our theoretical predictions, PathCond demonstrates improved convergence and generalization performance at small to moderate learning rates, where proper initialization plays a critical role in training stability. For the smallest learning rate ($lr = 10^{-4}$), we extend training to 500 epochs to observe convergence behavior, while other configurations use 128 epochs.

The results confirm that PathCond’s advantages are most pronounced in regimes where our theoretical assumptions hold, with performance converging to baseline as learning rates increase and optimization dynamics begin to dominate over initialization effects.

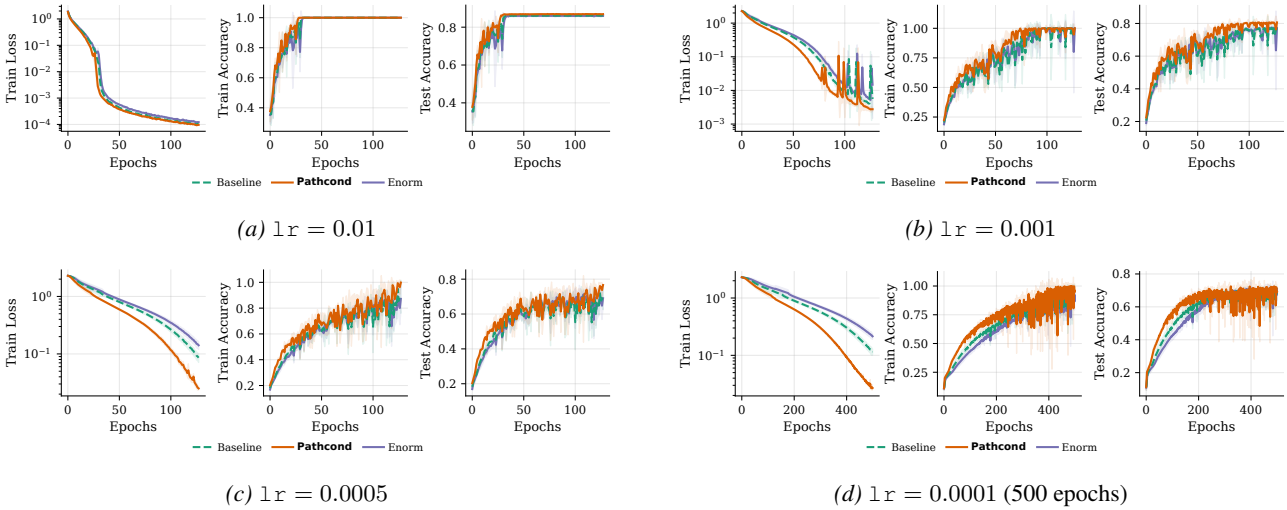


Figure 7. Training dynamics across different learning rates.

M. Additional Experiments for Section 5.3

We provide complementary experiments for Section 5.3, exploring the impact of learning rate on the relationship between varying-width architectures and required rescaling adjustments.

Figure 8 presents the final training loss and rescaling magnitudes across different compression factors for three learning rates. Consistent with our theoretical framework, the required rescaling magnitude increases with architectural width variation (higher compression factors) across all learning rates.

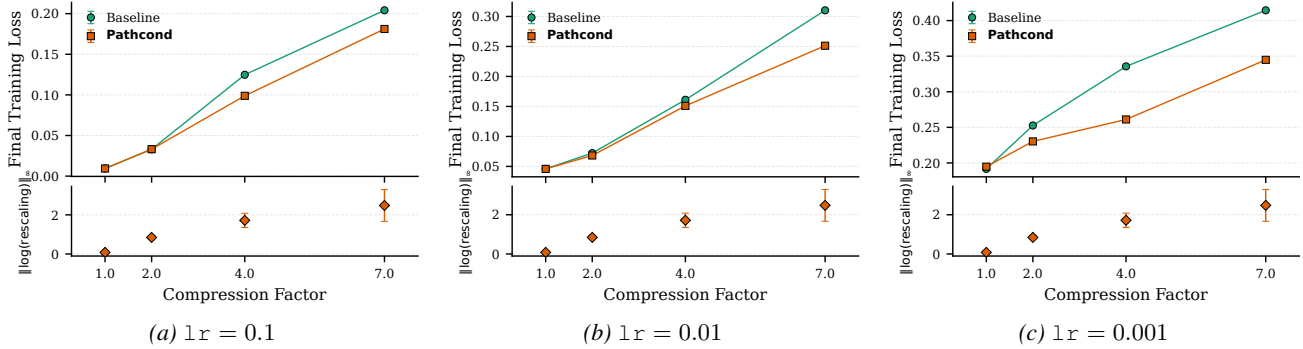


Figure 8. Final training loss (top) and rescaling magnitude (bottom) across compression factors for different learning rates.

N. ENorm : Experimental Setup

We describe the ENorm hyperparameter choices used in our comparisons. ENorm (Stock & Gribonval, 2023) rescales network weights at regular intervals to minimize a weighted sum of per-layer norms,

$$\sum_{\ell} c_{\ell} \|W_{\ell}\|_p^p$$

where the depth-dependent coefficient c_{ℓ} affects each layers. We use the default value $p = 2$, so ENorm minimizes the sum of squared ℓ_2 norms across layers. We set $c = 1$, which removes the depth penalty and treats all layers uniformly; as noted by the original authors, values of c at or slightly above 1 generally yield the best results.

ENorm can be applied every $k \geq 1$ SGD iterations. Following the recommendation of the original authors, we apply one ENorm cycle after each SGD iteration ($k = 1$).

For networks with BatchNorm layers, we follow the recommendation of the authors and exclude BatchNorm parameters from the rescaling cycle, applying ENorm to the remaining weights only—consistently with how PathCond handles BatchNorm.

In summary, all ENorm results in this paper use the default configuration: $p = 2$, $c = 1$, one rescaling cycle per SGD iteration, BatchNorm layers excluded.